ASYMPTOTIC AND NUMERICAL ANALYSIS OF DELAY-COUPLED MICROBUBBLE OSCILLATORS

A Dissertation

Presented to the Faculty of the Graduate School

of Cornell University

in Partial Fulfillment of the Requirements for the Degree of

Doctor of Philosophy

by

Christoffer R. Heckman

August 2012

ASYMPTOTIC AND NUMERICAL ANALYSIS OF DELAY-COUPLED MICROBUBBLE OSCILLATORS

Christoffer R. Heckman, Ph.D.

Cornell University 2012

Two vibrating bubbles submerged in a fluid influence each others' dynamics via sound waves in the fluid. Due to finite sound speed, there is a delay between one bubble's oscillation and the other's. This scenario is treated in the context of coupled nonlinear oscillators with a delay coupling term. It has previously been shown that with sufficient time delay, a supercritical Hopf bifurcation may occur for motions in which the two bubbles are in phase. In this work, we further examine the bifurcation structure of the coupled microbubble equations, including analyzing the sequence of Hopf bifurcations that occur as the time delay increases, as well as the stability of this motion for initial conditions which lie off the in-phase manifold. We show that in fact the synchronized, oscillating state resulting from a supercritical Hopf is attracting for such general initial conditions. The existence of a Hopf-Hopf bifurcation is also identified, and studied through an analogous system and the use of center manifold reductions. This procedure replaces the original DDE with four first-order ODEs, an approximation valid in the neighborhood of the Hopf-Hopf bifurcation. Analysis of the resulting ODEs shows that two separate periodic motions (limit cycles) and an additional quasiperiodic motion are born out of the Hopf-Hopf bifurcation. The analytical results are shown to agree with numerical results obtained by applying the continuation software package DDE-BIFTOOL to the original DDE.

BIOGRAPHICAL SKETCH

The author was born on February 3, 1986 in Orange County, California to Marilyn Heckman and Roger Heckman. The author attended the University of California at Berkeley where he conducted research with Prof. Andrew J. Szeri and obtained a Bachelor of Science degree in Mechanical Engineering in May, 2008. Cornell University's College of Engineering offered him an Olin Fellowship, which he accepted for study in the Department of Theoretical and Applied Mechanics. During his first year, he won a National Science Foundation Graduate Research Fellowship, which supported him for the remainder of his graduate work. The author went on to complete his Ph.D. in August of 2012.

This document is dedicated to the Department formerly known as Theoretical and Applied Mechanics.

ACKNOWLEDGEMENTS

I would like to thank my advisor, Richard Rand for his patience and for his help when I needed it, and for my independence when I didn't. I would also like to thank my minor advisors: Paul Steen for his always-helpful attitude and education in new methods, and Steve Strogatz for his generosity as a mentor and a teacher. Additionally, thanks go to John Guckenheimer, who has been especially formative in my education in dynamical systems and with whom conversations have always left me both energized and enlightened, and Herbert Hui, who has been both a good friend and a mentor.

I would also like to acknowledge the generous support of the National Science Foundation through a Graduate Research Fellowship. Because of their support I was able to continually benefit from the excellent teaching of many different instructors across departments, new research methods that involved both steep learning curves and great rewards, and, when time permitted, an exciting four years in gorgeous Ithaca. As required by the Foundation, I note here that any opinions, findings and conclusions or recommendations expressed in this publication are those of the author and do not reflect those of the National Science Foundation. In addition, I wish to acknowledge the financial support given to me by Cornell University through a Teaching Assistantship, an Instructorship, and an Olin Fellowship.

I would like to thank my twin brother Devin for always encouraging me to take the road less traveled if that was where I thought I would be happy. I would also like to thank my mother and the rest of my family for their encouragement throughout my twenty years of education.

TABLE OF CONTENTS

LIST OF TABLES

LIST OF FIGURES

CHAPTER 1

INTRODUCTION

This research pushes forward the base of knowledge on two fronts: the understanding of microbubble oscillators, and that of time-delay systems. Delay in dynamical systems is exhibited whenever the system's behavior is dependent at least in part on its history. Many technological and biological systems are known to exhibit such behavior; coupled laser systems, high-speed milling, population dynamics and gene expression are some examples of delayed systems. This work treats a new application of delay-differential equations, that of a microbubble cloud under acoustic forcing. This work is motivated by medical applications, where microbubbles are used in the noninvasive, localized delivery of drugs. In this process, microbubbles can either be filled with or their surfaces coated with drugs which work best locally. The microbubbles are propagated to the target site and collapsed by a strong ultrasound wave [20],[10],[15]. Full understanding of the behavior of systems of coupled microbubbles involves taking into account the speed of sound in the liquid, which will lead to a delay in induced pressure waves between the bubbles in a cloud.

In this vein, Chapter 2 will introduce the differential delay equations associated with microbubbles, and investigate a dynamical object named the "in-phase mode" for study of the physical problem via the theory of coupled oscillators. Here, a perturbation technique known as Lindstedt's Method is applied to characterize particular motions of interest. Chapter 3 will examine the stability of motions that bifurcate from the equilibria of these equations via the use of the two-variable expansion method and analysis of linear variational equations. Chapter 4 describes a codimension-2 bifurcation that occurs in the system via

the use of center manifold reductions on an analogous system. Finally, Chapter 5 is a summary of the conclusions of this research and consideration of future work.

1.1 Previous Work on Microbubbles

Previous work on bubbles has been steeped in the analysis of acoustic vibrations couched in physics. The first analysis in bubble dynamics was made by Rayleigh [35]. While in his work he considered an incompressible fluid with a constant background pressure, differential equation models of bubble dynamics in a compressible fluid with time-dependent background pressure were studied by, e.g., Plesset [29], Gilmore [16], Plesset and Prosperetti [30], and by Joseph Keller and his associates [22],[23], as well as many contemporaries including, for instance, Lauterborn [26] and Szeri [36],[38]. The main object of these studies has been the so-called Rayleigh-Plesset Equation, which governs the radius of a spherical bubble in a compressible fluid:

$$(\dot{a} - c)\left(a\ddot{a} + \frac{3}{2}\dot{a}^2 - \Delta\right) - \dot{a}^3 + a^{-1}\left(a^2\Delta\right)^{\cdot} = 0 \tag{1.1}$$

Here, $\Delta = \rho^{-1}\left(p(a) - p_0\right)$, where ρ is the density of the liquid, and p_0 is the far-field liquid pressure. The pressure $p(a)$ inside the bubble is calculated using the adiabatic relation $p(a) = k\left(\frac{4\pi}{3}a^3\right)^{-\gamma}$, where k is determined by the quantity and type of gas in the bubble and γ is the adiabatic exponent of the gas. Next, we nondimensionalize eq.(1.1) by setting

$$a = \tilde{a}\,k_a, \quad t = \tilde{t}\,k_t, \quad \text{and} \quad c = \tilde{c}(\rho/p_0)^{-1/2} \tag{1.2}$$

where

$$k_a = (3/(4\pi))^{1/3}(k/p_0)^{1/(3\gamma)}, \qquad k_t = k_a(\rho/p_0)^{1/2} \tag{1.3}$$

and obtain the dimensionless equation [22]:

$$(\dot{a} - c)\left(a\ddot{a} + \frac{3}{2}\dot{a}^2 - a^{-3\gamma} + 1\right) - \dot{a}^3 - (3\gamma - 2)\, a^{-3\gamma}\dot{a} - 2\dot{a} = 0 \tag{1.4}$$

where we have dropped the tildes on t, a and c for convenience.

Eq.(1.4) has an equilibrium solution at

$$a = a_e = 1 \tag{1.5}$$

To determine its stability, we set $a = a_e + x = 1 + x$ and linearize about $x = 0$, giving:

$$c\ddot{x} + 3\gamma\dot{x} + 3c\gamma x = 0 \tag{1.6}$$

Since c and γ are positive-valued parameters, eq.(1.6) corresponds to a damped linear oscillator, which tells us that the equilibrium (1.5) is stable.

1.2 Multiple Bubbles

Eq. (1.4) applies only to a single bubble submerged in a fluid field. If there are multiple bubbles submerged, then the bubbles become coupled by the pressure waves induced in the liquid. Therefore, eq. (1.4) no longer has the right-hand side equal to zero, but in fact will be driven by some coupling function. This system is illustrated in Figure 1.1.

With the introduction of a second bubble, the system under study becomes

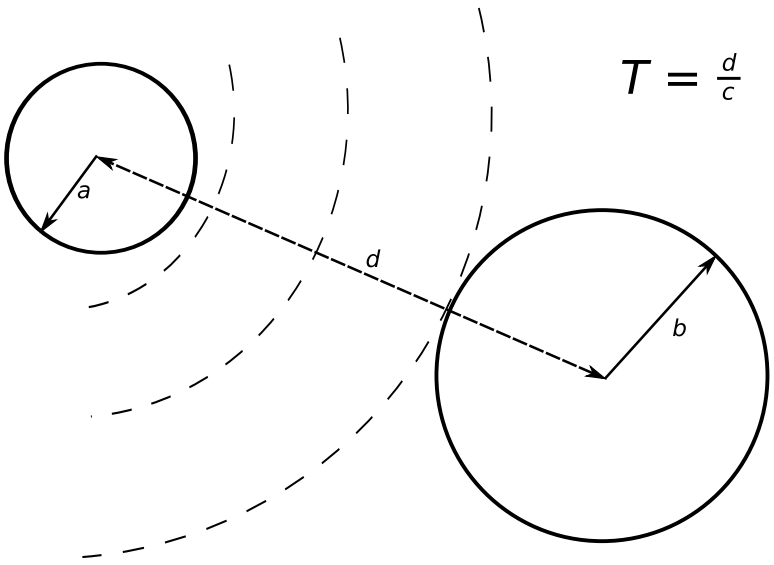

Figure 1.1: Two bubbles submerged in a liquid. Note that bubble b also influences bubble a with an induced acoustic wave. Delay $T = d/c$ where d is the distance between bubbles and c is sound speed.

more complex, with the compressibility of the fluid giving rise to a time delay in the coupling function between the two bubbles:

$$\begin{aligned}(\dot{a}-c)\left(a\ddot{a}+\frac{3}{2}\dot{a}^2-a^{-3\gamma}+1\right)-\dot{a}^3-(3\gamma-2)\,a^{-3\gamma}\dot{a}-2\dot{a}&=Pf(b(t-T))\\(\dot{b}-c)\left(b\ddot{b}+\frac{3}{2}\dot{b}^2-b^{-3\gamma}+1\right)-\dot{b}^3-(3\gamma-2)\,b^{-3\gamma}\dot{b}-2\dot{b}&=Pf(a(t-T))\end{aligned} \tag{1.7}$$

The preponderance of previous work has neglected the time-delay T, thereby reducing eqs. (1.7) to a standard nonlinear system of differential equations without delay. In these studies, very sophisticated patterns of bubble behavior have been discovered. For instance, assume that bubbles a and b have equilibrium bubble radii a_0 and b_0 respectively, and resonant frequencies ω_a and ω_b respectively. Without loss of generality, assume $a_0 < b_0$; a study of the reso-

nant frequencies of eq. (1.4) yields that $\omega_b < \omega_a$. In this case, if an acoustic driver forces both of the bubbles with frequency ω_{ext}, Harkin et *al* [19], then

$$\omega_{ext} < \omega_b \Rightarrow \quad \text{bubbles oscillate out of phase} \tag{1.8}$$

$$\omega_b < \omega_{ext} < \omega_a \Rightarrow \quad \text{bubbles oscillate in phase} \tag{1.9}$$

$$\omega_a < \omega_{ext} \Rightarrow \quad \text{bubbles oscillate out of phase} \tag{1.10}$$

Other works have studied the equation that governs translational dynamics of bubbles in a fluid [36],[38]. These have built upon previous work, asserting that bubbles oscillating in phase tend to be attracted to one another. Experimental work as accomplished by Yamakoshi et al. [41] has corroborated this finding. These works have not, however investigated the effect of delay on the coupled bubble system.

In the following chapters, the Rayleigh-Plesset Equation is studied with the effect of delay coupling as described above. Perturbation and numerical methods as well as analogous systems are used in order to examine the behavior of the equations near bifurcations, and to lay out the stability of oscillatory motions in the system.

CHAPTER 2

THE RAYLEIGH-PLESSET EQUATION WITH DELAY COUPLING

2.1 Two Coupled Bubble Oscillators

In this chapter we consider the dynamics of a system of two coupled bubble oscillators, each of the form of eq.(1.4), with delay coupling. Manasseh et al. [28] have studied coupled bubble oscillators without delay. The source of the delay comes from the time it takes for the signal to travel from one bubble to the other through the liquid medium which surrounds them. Adding the coupling terms used in [28], the governing eqs. of the bubble system are:

$$(\dot{a}-c)(a\ddot{a}+\frac{3}{2}\dot{a}^2-a^{-3\gamma}+1)-\dot{a}^3-(3\gamma-2)a^{-3\gamma}\dot{a}-2\dot{a} = P\dot{b}(t-T) \tag{2.1}$$

$$(\dot{b}-c)(b\ddot{b}+\frac{3}{2}\dot{b}^2-b^{-3\gamma}+1)-\dot{b}^3-(3\gamma-2)b^{-3\gamma}\dot{b}-2\dot{b} = P\dot{a}(t-T) \tag{2.2}$$

where T is the delay and P is a coupling coefficient. Here we have omitted coupling terms of the form $P_1 b(t-T)$ and $P_1 a(t-T)$ from eqs. (1.7), where P_1 is a coupling coefficient [28].

The system (2.1),(2.2) possesses an invariant manifold called the *in-phase manifold* given by $a = b$, $\dot{a} = \dot{b}$. A periodic motion in the in-phase manifold is called an *in-phase mode.* The dynamics of the in-phase mode are governed by the equation [7]:

$$(\dot{a}-c)\left(a\ddot{a}+\frac{3}{2}\dot{a}^2-a^{-3\gamma}+1\right)-\dot{a}^3-(3\gamma-2)\,a^{-3\gamma}\dot{a}-2\dot{a} = P\dot{a}(t-T) \tag{2.3}$$

This equation has the equilibrium $a = a_e = 1$. To determine the stability of this equilibrium, we set $a = a_e + x = 1 + x$ and linearize about $x = 0$, giving:

$$c\ddot{x} + 3\gamma\dot{x} + 3c\gamma x = -P\dot{x}(t - T) \tag{2.4}$$

Before proceeding with an analytical treatment of eq. (2.4), we use the MATLAB function `dde23` to numerically integrate (2.4). We choose the following dimensionless parameters based on the papers by Keller et al.:

$$c = 94, \qquad \gamma = \frac{4}{3}, \qquad P = 10 \tag{2.5}$$

Results of the numerical integration for linearized eq. (2.4) are shown in Figures A.1, A.2.

Inspection of Figures A.1, A.2 reveals that the equilibrium $a = 1$ loses its stability as the delay T is increased through a critical value T_{cr}. Associated with this periodic motion is its frequency ω_{cr}. From Figures A.1, A.2 we obtain the following approximate values for T_{cr} and ω_{cr}:

$$T_{cr} \approx 1, \qquad \omega_{cr} \approx 2 \tag{2.6}$$

Eq. (2.4) is a linear differential-delay equation. To solve it, we set $x = \exp \lambda t$ (see [33]), giving

$$c\lambda^2 + 3\gamma\lambda + 3c\gamma = -P\lambda \exp -\lambda T \tag{2.7}$$

We seek the smallest value of delay $T = T_{cr}$ which causes instability. This will correspond to imaginary values of λ. Thus we substitute $\lambda = i\omega$ in eq.(2.7)

giving two real equations for the real-valued parameters ω and T:

$$P\omega \sin \omega T = c(\omega^2 - 3\gamma) \tag{2.8}$$

$$P\omega \cos \omega T = -3\gamma\omega \tag{2.9}$$

Eq.(2.9) gives

$$\omega T = \arccos\left(\frac{-3\gamma}{P}\right) \tag{2.10}$$

whereupon eq.(2.8) becomes

$$\omega^2 - \frac{\sqrt{P^2 - 9\,\gamma^2}\,\omega}{c} - 3\,\gamma = 0 \tag{2.11}$$

from which we obtain

$$\omega_{cr} = \frac{\sqrt{P^2 - 9\,\gamma^2 + 12\,c^2\,\gamma} + \sqrt{P^2 - 9\,\gamma^2}}{2\,c} \tag{2.12}$$

which, when combined with (2.10), gives

$$T_{cr} = \frac{2\,c\,\arccos\left(-\frac{3\,\gamma}{P}\right)}{\sqrt{P^2 - 9\,\gamma^2 + 12\,c^2\,\gamma} + \sqrt{P^2 - 9\,\gamma^2}} \tag{2.13}$$

For the parameters of eq.(2.5), eqs.(2.12),(2.13) give

$$T_{cr} = 0.9673, \qquad \omega_{cr} = 2.0493 \tag{2.14}$$

which agree with the simulations in Figures A.1, A.2 , cf. eq.(2.6).

Eq.(2.13) shows that a necessary condition for instability is that the coupling parameter P must satisfy the inequality:

$$P > 3\gamma \tag{2.15}$$

Eq.(2.13) gives that as $P \to 3\gamma$, $T_{cr} \to \frac{\pi}{\sqrt{3\gamma}} = 1.622$ for $\gamma = \frac{4}{3}$. Figure A.3 shows a plot of T_{cr} as a function of P for parameters $c = 94$ and $\gamma = \frac{4}{3}$, from eq.(2.13). Therefore, for instability of the origin we need both $P > 3\gamma$ and $T > T_{cr}$.

This type of linear DDE analysis of a system of two bubbles has been presented in previous works by other investigators [25],[11]. Note that these results are unrealistic in the sense that unbounded behavior is predicted in the unstable case. The original nonlinear eq.(2.3) however predicts a bounded periodic motion for $T > T_{cr}$. See Figures A.4, A.5 where eq.(2.3) has been numerically integrated. The periodic motion has been born in a Hopf bifurcation [33].

In [7], Rand and Heckman have applied second order averaging [34],[31] to the nonlinear bubble eq.(2.3). The analysis assumed small delay. The same assumption of small delay was made by Wirkus and Rand [39], where first order averaging was used to study the dynamics of two van der Pol oscillators with delay coupling. In the present work we go beyond [7], and use large delay, perturbing off of T_{cr}. As we show next, we are able to analytically predict the amplitude of the limit cycle in Figure 2.1, for example.

2.2 Perturbations

As the time delay T is increased through T_{cr}, a pair of roots of the characteristic equation (2.7) for the linearized system (2.4) will cross the imaginary axis with zero real part. As the fixed point at the origin loses hyperbolicity, it will undergo

a Hopf bifurcation—and as a result, a limit cycle will be born. This limit cycle will start with zero amplitude and will grow as T is further increased. The relationship between the amplitude of the limit cycle and the value of T may be obtained through use of singular perturbation theory.

The method used here is known as Lindstedt's Method [33], a technique employed to approximate solutions in weakly nonlinear systems by eliminating secular terms. To begin, we perturb eq. (2.3) slightly from its equilibrium position by introducing a variable x, which tracks the deviation from equilibrium (recall eq. (1.5)):

$$a(t) = 1 + \epsilon x(t) \tag{2.16}$$

Inserting eq. (2.16) into the in-phase mode eq. (2.3) yields

$$\begin{aligned}(\epsilon\dot{x} - c)\left(\epsilon\ddot{x}(\epsilon x + 1) + \frac{3}{2}(\epsilon\dot{x})^2 - (\epsilon x + 1)^{-4} + 1\right) - (\epsilon\dot{x})^3 \\ -2\epsilon\dot{x}\left((\epsilon x + 1)^{-4} + 1\right) = \epsilon P\dot{x}_d\end{aligned} \tag{2.17}$$

where we have taken $\gamma = 4/3$. Note that for clarity we have redefined $x_d = x(t - T)$. Next, since ϵ is a small parameter, we take the Taylor Series of eq. (2.17) to obtain an expression for $\ddot{x}$ in powers of ϵ:

$$\begin{aligned}\ddot{x} \;=\; & -\frac{4xc + 4\dot{x} + P\,\dot{x}_d}{c} \\ & + \frac{\left(28x^2 - 3\dot{x}^2\right)c^2 + (24\,\dot{x} + 2P\dot{x}_d)\,xc - 8\dot{x}^2 - 2P\dot{x}_d\dot{x}}{2c^2}\epsilon \\ & - \frac{\left(68x^3 - 3\dot{x}^2x\right)c^3 + \left((64\dot{x} + 2P\dot{x}_d)\,x^2 + 2\dot{x}^3\right)c^2 - \left(24\dot{x}^2 + 2P\dot{x}_d\dot{x}\right)xc + 8\dot{x}^3 + 2P\dot{x}_d\dot{x}^2}{2c^3}\epsilon^2\end{aligned} \tag{2.18}$$

Note that in eq. (2.18), the $O(\epsilon)$ and $O(\epsilon^2)$ terms are all quadratic and cubic in x, respectively. This relationship will be used later in the process of Lindstedt.

We now introduce another asymptotic series that redefines time and builds a frequency-amplitude relationship into the limit cycle:

$$\tau = \Omega t \qquad \Omega = \omega_{cr} + \epsilon^2 k_2 + \dots \tag{2.19}$$

Now is the pivotal point at which we perturb off of the critical delay. This is done to eventually retrieve an asymptotic approximation for the amplitude of the limit cycle past the Hopf bifurcation. In order to accomplish this, we set

$$T = T_{cr} + \epsilon^2 \mu \tag{2.20}$$

in eq. (2.18), bearing in mind eq. (2.19). This step is pivotal since we are not perturbing the system for small delay, but rather for small deviations from T_{cr}, as calculated from the linear analysis eq. (2.13). Perturbing as such while changing the variable with respect to which we are differentiating will for instance transform terms such as

$$\begin{aligned} P\dot{x}(t-T) &= P\Omega x'(\tau - \Omega T) \\ &= P(\omega_{cr} + \epsilon^2 k_2) \underbrace{x'\left(\tau - \omega_{cr}T_{cr} - \epsilon^2\left(\omega_{cr}\mu + k_2 T_{cr}\right) + \dots\right)}_{\text{Taylor expand about } \tau - \omega_{cr}T_{cr}} \\ &= P\omega_{cr}x'_{d,cr} - P\epsilon^2\left(-k_2 x'_{d,cr} + \omega_{cr}\left(\omega_{cr}\mu + k_2 T_{cr}\right)x''_{d,cr}\right) + \dots \end{aligned}$$

where $(\cdot)'$ denotes differentiation with respect to τ and $x_{d,cr} = x(\tau - \omega_{cr}T_{cr})$, due to the change of variables (2.19). Other terms in eq. (2.18) have similar expansions resulting from the perturbation method.

As a final step in the perturbation method, the solution $x(\tau)$ is expanded in a series:

$$x(\tau) = x_0(\tau) + \epsilon x_1(\tau) + \epsilon^2 x_2(\tau) \tag{2.21}$$

Therefore

$$x(\tau - \omega_{cr}T_{cr}) = x_0(\tau - \omega_{cr}T_{cr}) + \epsilon x_1(\tau - \omega_{cr}T_{cr}) + \epsilon^2 x_2(\tau - \omega_{cr}T_{cr}) \tag{2.22}$$

Using eqs. (2.21)-(2.22), together with the perturbations in eqs. (2.20), (2.19), the Taylor series expansion in eq. (2.18) may be equated for the distinct orders of ϵ. This yields three equations ($O(1)$, $O(\epsilon)$, and $O(\epsilon^2)$):

$$L(x_0) = 0 \tag{2.23}$$

$$L(x_1) = -\frac{1}{2c^2}((3x_0'2c^2 + 8x_0'^2 + 2Px_{0d,cr}'x_0')\omega_{cr}^2 + ((-24x_0' - 2Px_{0d,cr}')cx_0)\omega_{cr} - 28c^2x_0^2) \tag{2.24}$$

$$\begin{aligned} L(x_2) = -\frac{1}{2c^3}((&-2T_{cr}x_{0d,cr}''Pc^2\omega_{cr} + (8x_0' + 2Px_{0d,cr}')c^2)k_2 \\ &+ (2x_0'^3c^2 + 8x_0'^3 + 2Px_{0d,cr}'x_0'^2)\omega_{cr}^3 + ((-3x_0'^2c^3 + (-24x_0'^2 - 2Px_{0d,cr}'x_0')c)x_0 \\ &+ 6x_1'x_0'c^3 - 2\mu x_{0d,cr}''Pc^2 + ((2x_{1d,cr}'P + 16x_1')x_0' + 2x_1'Px_{0d,cr}')c)\omega_{cr}^2 \\ &+ ((64x_0' + 2Px_{0d,cr}')c^2x_0^2 + (-2x_{1d,cr}'P - 24x_1')c^2x_0 + (-24x_1x_0' - 2x_1Px_{0d,cr}')c^2)\omega_{cr} \\ &+ 68c^3x_0^3 - 56x_1c^3x_0 - 2c^3k_2\omega_{cr}x_0'') \end{aligned} \tag{2.25}$$

where

$$L(x_i) = \omega_{cr}^2x_i'' + \frac{4\omega_{cr}}{c}x_i' + 4x_i + \frac{P\omega_{cr}}{c}x_{id,cr}$$

Eq. (2.23) has the solution

$$x_0(\tau) = A\sin\tau \tag{2.26}$$

Inserting eq. (2.26) in eq. (2.24) and using $x_{0d,cr} = A\sin(\tau - \omega_{cr}T_{cr})$ gives

$$
\begin{aligned}
L(x_1) =& \frac{A^2}{2c^2}\left(P\omega_{\rm cr}c\cos(T_{\rm cr}\omega_{\rm cr}) - P\omega_{\rm cr}^2\sin(T_{\rm cr}\omega_{\rm cr}) + 12\omega_{\rm cr}c\right)\sin 2\tau \\
&- \frac{A^2}{2c^2}\left(P\omega_{\rm cr}^2\cos(T_{\rm cr}\omega_{\rm cr}) + 4\omega_{\rm cr}^2 + \frac{3}{2}c^2\omega_{\rm cr}^2 + P\omega_{\rm cr}\sin(T_{\rm cr}\omega_{\rm cr}) - 14c^2\right)\cos 2\tau \\
&- A^2\left(\frac{\omega_{\rm cr}^2 P\cos(T_{\rm cr}\omega_{\rm cr})}{2c^2} + \frac{2\omega_{\rm cr}^2}{c^2} + \frac{3\omega_{\rm cr}^2}{4} - \frac{P\omega_{\rm cr}\sin(T_{\rm cr}\omega_{\rm cr})}{2c} - 7\right) \qquad (2.27)
\end{aligned}
$$

Note that eq. (2.27) has no secular terms since , as mentioned above, in eq. (28) the $O(\epsilon)$ terms are all quadratic. Next we look for a solution to eq. (2.27) as:

$$x_1(\tau) = B\sin 2\tau + C\cos 2\tau + D \qquad (2.28)$$

where the coefficients B,C and D are listed in the Appendix. Substituting eqs. (2.26), (2.28), (A.1), (A.2) and (A.3) in eq. (2.25) gives

$$L(x_2) \quad = \quad \Gamma_1\cos\tau + \Gamma_2\sin\tau + NRT \qquad (2.29)$$

where Γ_1, Γ_2 are terms depending on $A, B, C, D, c, \omega_{cr}, T_{cr}, k_2$ and μ. In eq. (2.29), NRT stands for non-resonant terms. Next we remove resonant terms by setting the coefficients $\Gamma_1 = \Gamma_2 = 0$. This yields expressions for the frequency shift k_2 and the amplitude A. These expressions are too long to list here (for example, the expression for k_2 has 154 terms when written in terms of μ, c, P, T_{cr} and ω_{cr}). For the parameters of eqs.(2.5),(2.14) we find:

$$k_2 = -1.4506\,\mu, \qquad\qquad A = 1.4523\ \sqrt{\mu} \qquad (2.30)$$

where μ is the detuning given by eq.(2.20).

A comparison of the perturbation method results and the numerical results are provided in Figure 2.1, below.

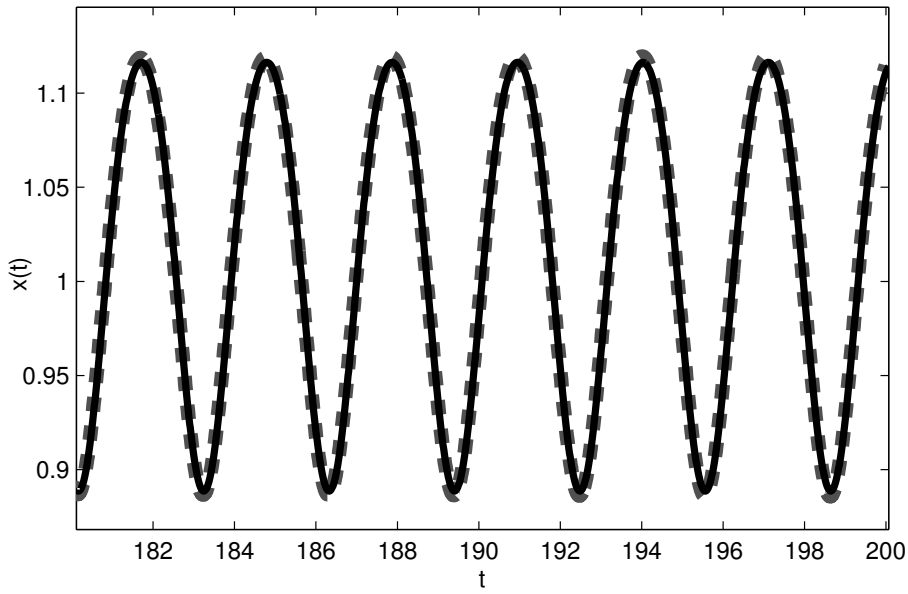

Figure 2.1: Perturbation results (solid line) compared against numerical integration (dashed line) of eq.(2.3) for the parameters of eq.(2.5) with delay $T = 0.98$.

2.3 Conclusion

In this chapter we have begun to explore the dynamics of two delay-coupled bubble oscillators, eqs.(2.1),(2.2), and in particular we have studied the dynamics of the in-phase mode, eq.(2.3). In a classic paper, Keller and Kolodner [22] showed that the uncoupled bubble oscillator (eq.(2.3) with $P = 0$) is conservative in the incompressible limit, and is damped if c is allowed to take on a finite value. Our study of the in-phase mode adds a delay feedback term to the system studied in [22]. We showed that the equilibrium can be made unstable if the delay is long enough and if the coupling coefficient P is large enough. This change in stability is accompanied by a Hopf bifurcation in which a stable periodic motion (a limit cycle) is born.

In particular, we investigated the stability of equilibrium in the in-phase mode through the use of the linear variational eq.(2.4). Analysis of the characteristic eq.(2.7) yielded closed form expressions for T_{cr} and ω_{cr}, eqs.(2.12),(2.13). For values of delay T which are slightly larger than T_{cr}, we used Lindstedt's method to second order in ϵ to obtain values for the frequency and amplitude of the limit cycle.

CHAPTER 3

STABILITY OF THE IN-PHASE MODE

3.1 Introduction

In this work we consider the dynamics of a system of two delay-coupled bubble oscillators. The bubbles are modeled by the Rayleigh-Plesset equation, featuring a coupling term that is delayed as a result of the finite speed of sound in the fluid. A drawing of the physical phenomenon under study is presented in Figure 1.1. Manasseh et al. [28] have studied coupled bubble oscillators without delay. The source of the delay comes from the time it takes for the signal to travel from one bubble to the other through the liquid medium which surrounds them. Adding the coupling terms used in [28], the governing equations of the bubble system are:

$$(\dot{a}-c)(a\ddot{a}+\frac{3}{2}\dot{a}^2-a^{-3\gamma}+1)-\dot{a}^3-(3\gamma-2)a^{-3\gamma}\dot{a}-2\dot{a} = P\dot{b}(t-T) \tag{3.1}$$

$$(\dot{b}-c)(b\ddot{b}+\frac{3}{2}\dot{b}^2-b^{-3\gamma}+1)-\dot{b}^3-(3\gamma-2)b^{-3\gamma}\dot{b}-2\dot{b} = P\dot{a}(t-T) \tag{3.2}$$

where T is the delay and P is a coupling coefficient. Here we have omitted coupling terms of the form $P_1 b(t-T)$ and $P_1 a(t-T)$ from eqs. (3.1), (3.2), where P_1 is a coupling coefficient [28]. Note that the equation follows the form explored by Keller et al. [22]:

Eqs. (3.1), (3.2) have an equilibrium solution at

$$a = a_e = 1, \quad b = b_e = 1 \tag{3.3}$$

Analyzing only bubble A, we may determine the stability of its equilibrium radius by setting $a = a_e + x = 1 + x$ and linearize about $x = 0$, giving:

$$c\ddot{x} + 3\gamma\dot{x} + 3c\gamma x + P\dot{x}(t - T) = 0 \tag{3.4}$$

Note that, since c and γ are positive-valued parameters, if delay were absent from the model ($T = 0$), then eq. (3.4) would correspond to a damped linear oscillator, which tells us that the equilibrium (3.3) would be stable. In the presence of delay, the characteristic equation must be solved to determine if any roots have positive real part.

3.2 Bifurcations of the In-Phase Mode

As studied previously [6], the system (3.1),(3.2) possesses an invariant manifold called the *in-phase manifold* given by $a = b$, $\dot{a} = \dot{b}$. A periodic motion in the in-phase manifold is called an *in-phase mode.* The dynamics of the in-phase mode are governed by the equation [7]:

$$(\dot{a} - c)\left(a\ddot{a} + \frac{3}{2}\dot{a}^2 - a^{-3\gamma} + 1\right) - \dot{a}^3 - (3\gamma - 2)\, a^{-3\gamma}\dot{a} - 2\dot{a} = P\dot{a}(t - T) \tag{3.5}$$

We analyze the equilibrium of this equation $a = a_e = 1$ for Hopf bifurcations, giving rise to oscillations. When Hopf bifurcations occur, there will be a change

in stability of the equilibrium point. To study the stability of the equilibrium point, we will analyze its linearization as provided in eq.(1.6). This equation is a linear differential-delay equation. To solve it, we set $x = \exp \lambda t$ (see [33]), giving

$$c\lambda^2 + 3\gamma\lambda + 3c\gamma = -P\lambda \exp -\lambda T \tag{3.6}$$

We seek the values of delay $T = T_{cr}$ which cause instability. This will correspond to imaginary values of λ. Thus we substitute $\lambda = i\omega$ in eq.(3.6) giving two real equations for the real-valued parameters ω and T:

$$P\omega \sin \omega T = c(\omega^2 - 3\gamma) \tag{3.7}$$

$$P\omega \cos \omega T = -3\gamma\omega \tag{3.8}$$

Note that these equations have infinitely many solutions, as anticipated by the transcendental form of eq. (3.6). In our previous work, only the first solution was studied. However, a further analysis of the bifurcation structure involves analyzing the full solution set to eqs. (3.7), (3.8). We choose the following dimensionless parameters based on the papers by Keller et al. when numerics are required:

$$c = 94, \quad \gamma = \frac{4}{3}, \quad P = 10 \tag{3.9}$$

The solutions to eq. (3.6) are then found to be:

$$\omega_\alpha = \frac{\sqrt{P^2 - 9\gamma^2 + 12c^2\gamma} + \sqrt{P^2 + 9\gamma^2}}{2c} \approx 2.0493 \Rightarrow$$
$$T_\alpha = \frac{\arccos\left(\frac{-3\gamma}{10}\right) + 2\pi n}{\omega_\alpha} \, (n \in \mathbb{Z}) \tag{3.10}$$

$$\omega_\beta = \frac{\sqrt{P^2 - 9\gamma^2 + 12c^2\gamma} - \sqrt{P^2 + 9\gamma^2}}{2c} \approx 1.9518 \Rightarrow$$
$$T_\beta = \frac{-\arccos\left(\frac{-3\gamma}{10}\right) + 2\pi m}{\omega_\beta} \; (m \in \mathbb{Z}) \tag{3.11}$$

Notice that, while there are only *two* frequencies ω_α, ω_β that solve the equations, each of them has an *infinite sequence* of T_α, T_β respectively that pairs with it as a solution. We will designate any delay T at which a Hopf bifurcation occurs as T_{cr}, independent of its corresponding frequency. Because of the solutions to eqs. (3.7), (3.8) there will be two infinite sequences of solutions that occur simultaneously. Each of the T_α, T_β delays correspond to Hopf bifurcations.

Using the numerical continuation package `DDE-BIFTOOL` [13], we present the amplitude of limit cycle oscillations that are born out of these sequences of Hopfs in Figure 3.1. Note that the first Hopf bifurcation is of T_α-type, followed by one of T_β type. The two limit cycles born out of these Hopf bifurcations grow until they reach a radius at which the two coalesce and annihilate one another in a saddle-node of periodic orbits. Until $T \approx 44$ in Figure 3.1, it can be seen that a T_α-type Hopf always precedes a T_β-type Hopf.

As T increases in Figure 3.1, this ordering is reversed at $T \approx 44$. Here, another T_α-type Hopf bifurcation occurs prior to the T_β-type Hopf. This generic exchange in order of the two sequences has as a degenerate case the possibility that the two Hopf bifurcations align exactly, resulting in a Hopf-Hopf bifurcation. This phenomenon has been studied previously by means of center manifold reductions [5]. A separate approach taken is to track the value of the real part of the eigenvalues; when there the real part is zero, there is a Hopf bifurcation.

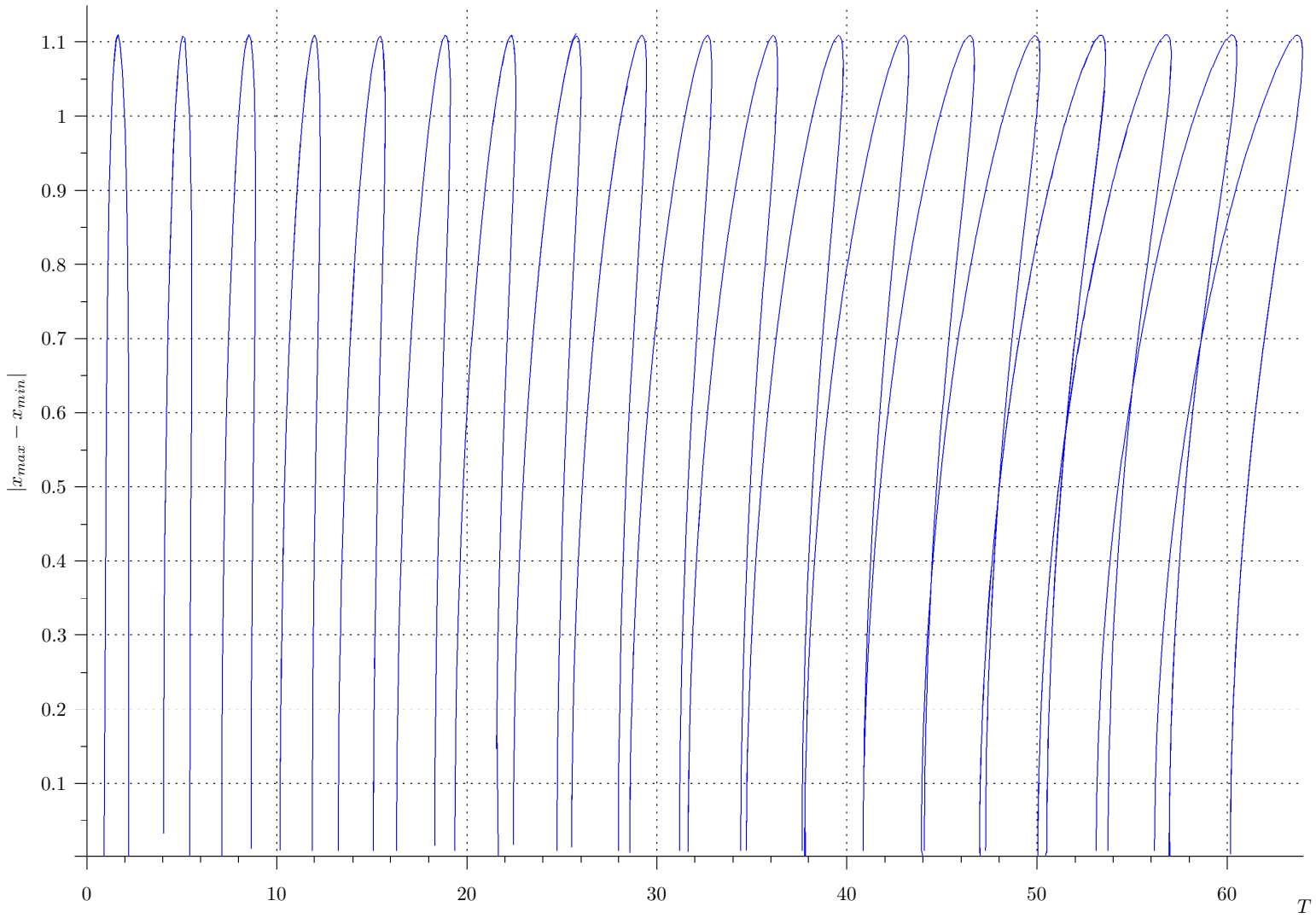

Figure 3.1: Numerical continuation of eq. (3.5) for the parameter values in eq. (3.9), with T as the continuation parameter.

Next, we further examine Figure 3.1 by characterizing representative regions of the figures. We recognize three distinct "regions" of qualitatively different behavior as the delay parameter increases. The first is presented in Figure 3.2, which exhibits a sequence first of T_α resulting in limit cycle growth, followed by the incidence of T_β which also spawns a limit cycle that meets the first Hopf curve in a saddle-node of periodic orbits. After the limit cycles are annihilated, the only invariant motion is the equilibrium point.

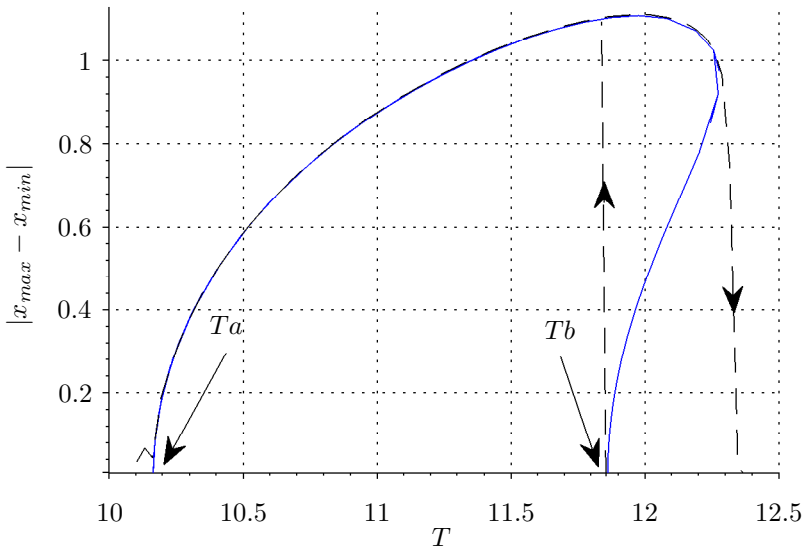

Figure 3.2: A T_α-type Hopf bifurcation followed by a T_β-type. Here, the Hopf points are situated such that there is still a region where, after the two limit cycles are annihilated, the equilibrium point regains stability. Solid lines correspond to continuation whereas dashed lines correspond to jumps which show the stability of solutions as determined by numerical integration.

The region presented in Figure 3.3 has the same bifurcation structure as that presented in Figure 3.2, except that the trailing T_β-type Hopf bifurcation occurs close enough to the next T_α bifurcation such that for any delay value, there exists two stable periodic motions.

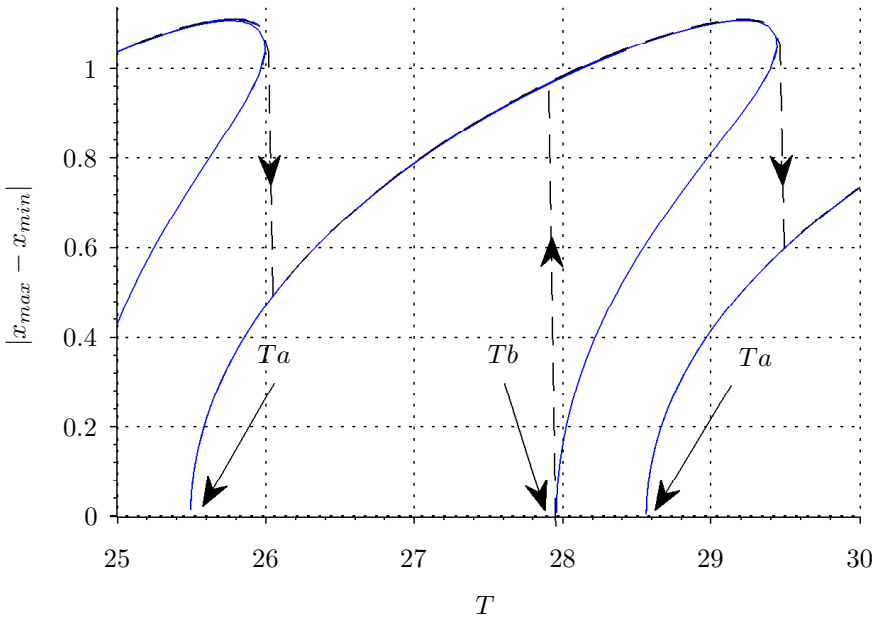

Figure 3.3: A T_α-type Hopf bifurcation followed by a T_β-type, but with at least two limit cycles coexisting with the equilibrium point continuously throughout the parameter range. Solid lines correspond to continuation whereas dashed lines correspond to jumps which show the stability of solutions as determined by numerical integration.

The region presented in Figure 3.4 presents sophisticated behavior that is explored in greater depth by the authors through the use of an analogous system and the center manifold reduction method [5]. Just prior to this region (as apparent in Figure 3.1), there is a reordering of the Hopf bifurcation sequence as a result of two T_α-type Hopfs occurring in a row at $T \approx 44$. This reordering is a possibility granted only by the infinite number of roots for λ in eq. (3.6) and the fact that eq. (3.5) is an infinite-dimensional dynamical system. As a result, the behavior in Figure 3.4 shows the Hopf curves apparently intersecting. It should be noted that each Hopf bifurcation occurs in its own two-dimensional center manifold, and these amplitude curves are only a projection of the dynamics of the system.

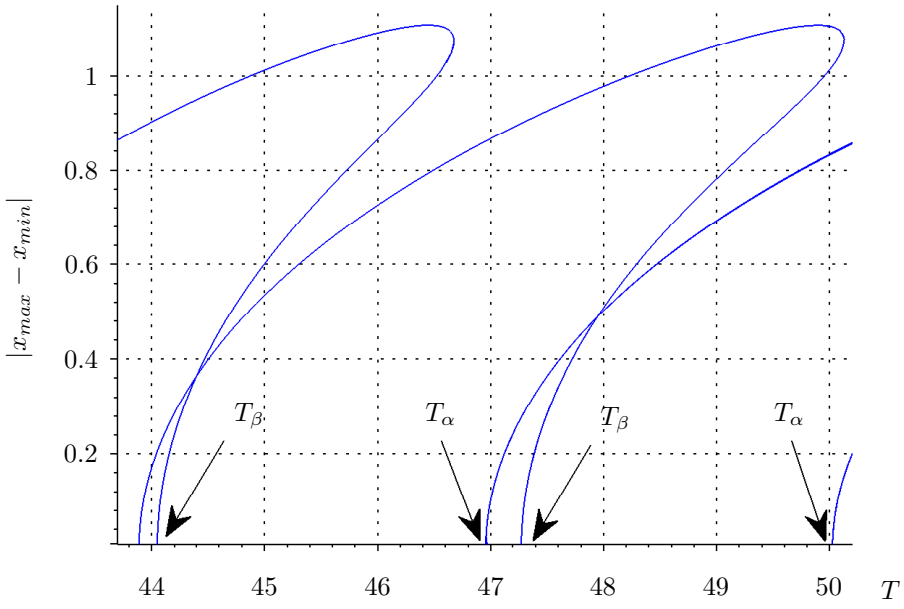

Figure 3.4: For larger delay, the Hopf curves appear to meet as a result the reordering of the Hopf points at $T \approx 44$. Solid lines correspond to continuation; the jumps have been omitted.

The primary focus of the forthcoming analysis is the case where the T_α- and T_β-type Hopfs follow each other in that order (i.e. regions corresponding to Figures 3.2 and 3.3).

The Hopf bifurcations may be further characterized by their criticality. To analyze whether the bifurcations are supercritical or subcritical, regular perturbations may be employed to characterize the motion of the associated eigenvalues. In particular, we begin with the characteristic eq. (3.6) and let $T = T_{cr} + \mu_1$. Next, we establish perturbations on the eigenvalue:

$$\lambda = i\omega_{\text{cr}} + K_1\mu_1 + iK_2\mu_1 \tag{3.12}$$

Table 3.1: Sequence of the first several T_α-type Hopf bifurcations and their corresponding values of K_1.

n	1	2	3	4	5	6	7
T_{cr}	0.9673	4.0332	7.0992	10.1651	13.2311	16.2970	19.3630
K_1	0.0979	0.0836	0.0701	0.0585	0.0488	0.0410	0.0346

That is, assume that $\Re(\lambda) = 0$ whenever $\mu_1 = 0$. Equating the real and imaginary parts of eq. (3.6) with consideration of eq. (3.12), and expanding for small μ_1 results in:

$$K_1\mu_1(-3c\omega_{\text{cr}}^2 + 3\gamma + 3c) = \mu_1(\cos(T_{\text{cr}}\omega_{\text{cr}})(-\omega_{\text{cr}}^2 P - K_2 T_{\text{cr}}\omega_{\text{cr}} P - K_1 P) + \sin(T_{\text{cr}}\omega_{\text{cr}})(K_1 T_{\text{cr}}\omega_{\text{cr}} P - K_2 P)) - \omega_{\text{cr}}\sin(T_{\text{cr}}\omega_{\text{cr}})P \tag{3.13}$$

$$-c\omega_{\text{cr}}^3 + K_2\mu_1(-3c\omega_{\text{cr}}^2 + 3\gamma + 3c) + (3\gamma + 3c)\omega_{\text{cr}} = \mu_1(\cos(T_{\text{cr}}\omega_{\text{cr}})(K_1 T_{\text{cr}}\omega_{\text{cr}} P - K_2 P) - \sin(T_{\text{cr}}\omega_{\text{cr}})(-\omega_{\text{cr}}^2 P - K_2 T_{\text{cr}}\omega_{\text{cr}} P - K_1 P)) - \omega_{\text{cr}}\cos(T_{\text{cr}}\omega_{\text{cr}})P \tag{3.14}$$

In solving for K_1, K_2 in terms of μ_1, we determine the "speed" at and direction in which the eigenvalues cross the imaginary axis. In particular, the sign of K_1 is of immediate interest; in particular, $K_1 > 0$ implies that the roots are moving from the left half-plane to the right half-plane, implying a stable origin becomes unstable. This is one of the conditions for a supercritical Hopf bifurcation.

Applying the conditions guaranteed by eqs. (3.10), (3.11) subsequently into the expression for K_1 in eq. (3.13) gives a long expression, for which we substitute in parameter values. For the first several ω_α-type Hopf bifurcations, the sequence of K_1 is provided in Table 3.1, whereas for the first several T_β-type Hopf bifurcations, the sequence of K_1 is provided in Table 3.2.

Table 3.2: Sequence of the first several T_β-type Hopf bifurcations and their corresponding values of K_1.

n	1	2	3	4	5	6	7
T_{cr}	2.2035	5.4226	8.6417	11.8608	15.0799	18.2990	21.5181
K_1	-0.0840	-0.0712	-0.0595	-0.0496	-0.0415	-0.0349	-0.0296

Given the exchange of stability that occurs at these Hopf bifurcations, we therefore conclude that the T_α values for delay correspond to supercritical Hopf bifurcations, whereas those corresponding to T_β correspond to subcritical bifurcations.

In Figure 3.5, we show the plot of $\Re(\lambda)$ vs. T for the first several solutions to the characteristic eq. (3.6). Note that in this figure, when $\Re(\lambda) = 0$, there is a Hopf bifurcation. Also, at $T \approx 44$, the reordering previously discussed results in the extinction of isolated regions where the equilibrium point regains stability. Figure 3.5 was generated using algebraic continuation in AUTO [12] [3].

3.3 Stability of the In-Phase Mode

In the previous section, we established that in response to an increase in delay T, there is a bifurcation structure which alternates between supercritical and subcritical Hopf bifurcations. We drew this conclusion by analyzing the stability of the origin and inferring the stability of the periodic motion after bifurcation. However, there is a direct way to approach the stability of the in-phase mode by means of perturbations [4].

The two-variable expansion method is a well-known procedure for analyz-

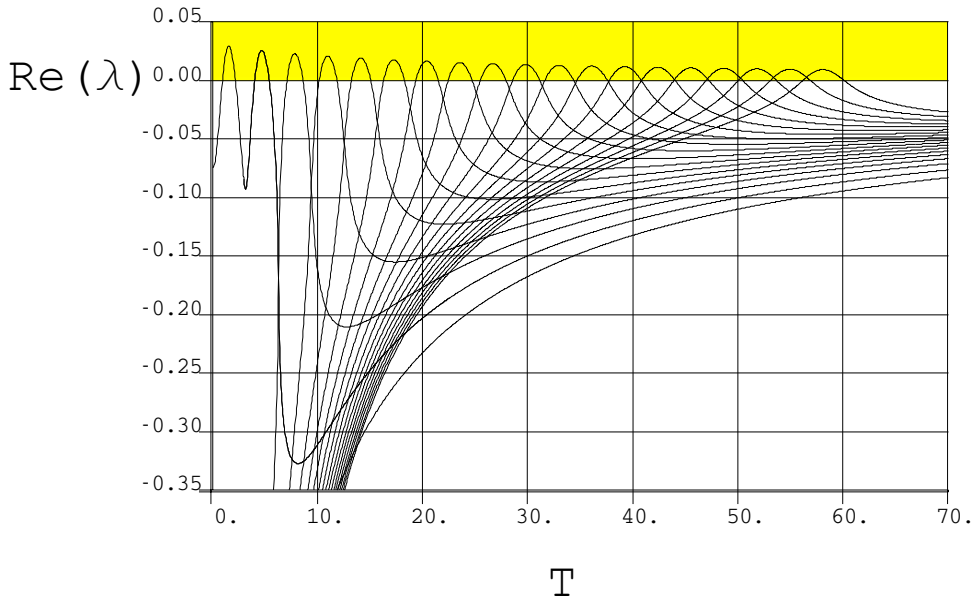

Figure 3.5: $\Re(\lambda)$ vs. T for the first several roots of characteristic eq. (3.6) generated by numerical continuation via AUTO, using parameters (3.9).

ing the amplitude and stability of limit cycles born in a Hopf bifurcation [33]. In a previous study, the authors performed second order averaging [7] on the system for small delay. The two variable method is analogous to the second-order averaging approach and both methods will generate a set of differential equations for the amplitude and frequency of the limit cycle, as well as the approach of solutions that start sufficiently close to the limit cycle.

To begin, we introduce two variables: one fast, another slow:

$$\xi = \Omega t \tag{3.15}$$

$$\eta = \epsilon^2 t \tag{3.16}$$

Note that we expand immediately to $O(\epsilon^2)$; this is necessary because the nonlinearities are of quadratic order. This expansion will result in the following

applications of the chain rule:

$$\begin{aligned}\frac{dx}{dt} &= \Omega\frac{\partial x}{\partial \xi} + \epsilon^2\frac{\partial x}{\partial \eta} \\ \frac{d^2x}{dt^2} &= \Omega^2\frac{\partial^2 x}{\partial \xi^2} + 2\Omega\epsilon^2\frac{\partial^2 x}{\partial \xi \partial \eta} + \epsilon^4\frac{\partial^2 x}{\partial \eta^2}\end{aligned} \tag{3.17}$$

Likewise, the time-delay term will also be affected by the chain rule [32]:

$$\dot{x}(t-T) = \Omega\frac{\partial x(\xi - \Omega T, \eta - \epsilon^2 T)}{\partial \xi} + \epsilon^2\frac{\partial x(\xi - \Omega T, \eta - \epsilon^2 T)}{\partial \eta} \tag{3.18}$$

We now introduce another asymptotic series that builds a frequency-amplitude relationship into the limit cycle:

$$\Omega = \omega_{\text{cr}} + \epsilon^2 k_2 \tag{3.19}$$

Now is the pivotal point at which we perturb off of the critical delay. This is done to eventually retrieve an asymptotic approximation for the dynamics of the system in the in-phase manifold past the Hopf bifurcation. In order to accomplish this, we set

$$T = T_{\text{cr}} + \epsilon^2 \mu_2 \tag{3.20}$$

The quantity ΩT may be expanded, dropping terms smaller than $O(\epsilon^2)$:

$$\Omega T = \omega_{\text{cr}} T_{\text{cr}} + \epsilon^2(\mu_2 \omega_{\text{cr}} + k_2 T_{\text{cr}}) \tag{3.21}$$

In the derivation that follows, the shorthand $x_{\mathrm{d}} = x(\xi - \omega_{\mathrm{cr}} T_{\mathrm{cr}}, \eta)$ is adopted [37]. We wish to expand eq. (3.18) taking into account eq. (3.21). To fully expand this delay term in terms of its constituent derivatives, we note that:

$$\begin{aligned}
\frac{d}{d\xi} x\left(\xi - \Omega T, \eta - \epsilon^2 T\right) &= \frac{d}{d\xi} x\left(\xi - (\omega_{\mathrm{cr}} + \epsilon^2 k_2)(T_{\mathrm{cr}} + \epsilon^2 \mu_2), \eta - \epsilon^2 (T_{\mathrm{cr}} + \epsilon^2 \mu_2)\right) + \dots \\
&= \frac{d}{d\xi} x(\xi - \omega_{\mathrm{cr}} T_{\mathrm{cr}} - \epsilon^2 (k_2 T_{\mathrm{cr}} + \mu_2 \omega_{\mathrm{cr}}), \eta - \epsilon^2 T_{\mathrm{cr}}) + \dots \\
&= \frac{d}{d\xi} x(\xi - \omega_{\mathrm{cr}} T_{\mathrm{cr}}, \eta) - \epsilon^2 (k_2 T_{\mathrm{cr}} + \mu_2 \omega_{\mathrm{cr}}) \frac{d^2}{d\xi^2} x(\xi - \omega_{\mathrm{cr}} T_{\mathrm{cr}}, \eta) \\
&\quad - \epsilon^2 T_{\mathrm{cr}} \frac{d^2}{d\xi d\eta} x(\xi - \omega_{\mathrm{cr}} T_{\mathrm{cr}}, \eta) + \dots
\end{aligned}$$

which we write as:

$$\frac{d}{d\xi} x\left(\xi - \Omega T, \eta - \epsilon^2 T\right) = x_{\mathrm{d}_\xi} - \epsilon^2 x_{\mathrm{d}_{\xi\xi}} (k_2 T_{\mathrm{cr}} + \mu_2 \omega_{\mathrm{cr}}) - \epsilon^2 T_{\mathrm{cr}} x_{\mathrm{d}_{\xi\eta}} + \dots$$

Therefore, the expansion for eq. (3.18) is:

$$\begin{aligned}
\dot{x}_d &= (\omega_{\mathrm{cr}} + \epsilon^2 k_2) x_\xi (t - T) + \epsilon^2 x_\eta (t - T) + \dots \\
&= (\omega_{\mathrm{cr}} + \epsilon^2 k_2)(x_{\mathrm{d}_\xi} - \epsilon^2 x_{\mathrm{d}_{\xi\xi}} (k_2 T_{\mathrm{cr}} + \mu_2 \omega_{\mathrm{cr}}) - \epsilon^2 T_{\mathrm{cr}} x_{\mathrm{d}_{\xi\eta}} + \dots) + \epsilon^2 x_{\mathrm{d}_\eta} + \dots \\
&= \omega_{\mathrm{cr}} x_{\mathrm{d}_\xi} - \epsilon^2 \left((\mu_2 \omega_{\mathrm{cr}}^2 + k_2 T_{\mathrm{cr}} \omega_{\mathrm{cr}}) x_{\mathrm{d}_{\xi\xi}} - k_2 x_{\mathrm{d}_\xi} + T_{\mathrm{cr}} \omega_{\mathrm{cr}} x_{\mathrm{d}_{\eta\xi}} - x_{\mathrm{d}_\eta}\right) + \dots
\end{aligned} \tag{3.22}$$

Next, the solution to the differential equation is expanded in powers of ϵ:

$$x(\xi, \eta) = x_0(\xi, \eta) + x_1(\xi, \eta) + x_2(\xi, \eta) + \cdots \tag{3.23}$$

Using eqs. (3.23), (3.22) along with the perturbations (3.17), (3.19), and (3.20), the Taylor series expansion of eq. (3.5) may be equated for the distinct orders of ϵ. This yields three equations ($O(1)$, $O(\epsilon)$, and $O(\epsilon^2)$):

$$L(x_0) = 0 \tag{3.24}$$

$$L(x_1) = \frac{1}{2c}\left((2\omega_{\mathrm{cr}}^3 x_{0_\xi} - 2c\omega_{\mathrm{cr}}^2 x_0)x_{0_{\xi\xi}} - 3c\omega_{\mathrm{cr}}^2 x_{0_\xi}^2 + 24\omega_{\mathrm{cr}} x_0 x_{0_\xi} + 20c x_0^2\right) \tag{3.25}$$

$$\begin{aligned} L(x_2) = &-(4c^3\omega_{\mathrm{cr}} x_{0_{\xi\eta}} + (2c^2 x_{0_\xi}^3 + 8x_{0_\xi}^3 + 2P x_{0\mathrm{d}_\xi} x_{0_\xi}^2)\omega_{\mathrm{cr}}^3 + ((-3x_0 x_{0_\xi}^2 + 6x_{1_\xi} x_{0_\xi})c^3 \\ &- 2Pc^2\mu_2 x_{0\mathrm{d}_{\xi\xi}} + (-24x_0 x_{0_\xi}^2 + (16x_{1_\xi} - 2P x_{0\mathrm{d}_\xi} x_0 + 2P x_{1\mathrm{d}_\xi})x_{0_\xi} + 2P x_{0\mathrm{d}_\xi} x_{1_\xi})c)\omega_{\mathrm{cr}}^2 \\ &+ ((4c^3 x_{0_{\xi\xi}} - 2PT_{\mathrm{cr}} x_{0\mathrm{d}_{\xi\xi}} c^2)k_2 + ((64x_0^2 - 24x_1)x_{0_\xi} - 24x_0 x_{1_\xi} + 2P x_{0\mathrm{d}_\xi} x_0^2 \\ &- 2P x_{1\mathrm{d}_\xi} x_0 - 2P x_{0\mathrm{d}_\xi} x_1 - 2P x_{0\mathrm{d}_{\xi\eta}} T_{\mathrm{cr}})c^2)\omega_{\mathrm{cr}} + (8x_{0_\xi} + 2P x_{0\mathrm{d}_\xi})c^2 k_2 \\ &+ (68x_0^3 - 56x_1 x_0)c^3 + (8x_{0_\eta} + 2P x_{0\mathrm{d}_\eta})c^2)/(2c^3) \end{aligned} \tag{3.26}$$

where

$$L(x_i) = \omega_{\mathrm{cr}}^2 x_{i_{\xi\xi}} + \frac{4\omega_{\mathrm{cr}}}{c} x_{i_\xi} + 4x_i + \frac{P\omega_{\mathrm{cr}}}{c} x_{i\mathrm{d}_\xi} \tag{3.27}$$

From (3.27) we see that $L(x_0) = 0$ can be solved for $x_{0\mathrm{d}_\xi}$, and using this, appearances of $x_{0\mathrm{d}}$ in eq.(3.25) have been replaced by non-delayed values of x_0, x_{0_ξ} and $x_{0_{\xi\xi}}$.

Eq. (3.24) has the solution

$$x_0(\xi, \eta) = A(\eta)\cos(\xi) + B(\eta)\sin(\xi) \tag{3.28}$$

Inserting eq. (3.28) into eq. (3.25) and expanding appropriately gives the result:

$$L(x_1) = \left(\frac{\omega_{cr}^3 - 12\omega_{cr}}{2c}(A^2 - B^2) + \frac{5\omega_{cr}^2 + 20}{2}AB\right)\sin(2\xi) + \left(\frac{5\omega_{cr}^2 + 20}{4}(A^2 - B^2) + \frac{12\omega_{cr} - \omega_{cr}^3}{c}AB\right)\cos(2\xi) - \left(\frac{\omega_{cr}^2 - 20}{4}\right)(A^2 + B^2) \tag{3.29}$$

Note that $L(x_1)$ has no secular terms since all $O(\epsilon)$ terms are quadratic, as expected. Eq.(3.25) has the solution:

$$x_1(\xi, \eta) = C(\eta)\cos(\xi) + D(\eta)\sin(\xi) + E(\eta)\cos(2\xi) + F(\eta)\sin(2\xi) + G(\eta) \tag{3.30}$$

where the coefficients C, D are arbitrary functions of η, and where E, F and G are known functions of A and B. We substitute eq. (3.30) for x_1 into eq. (3.26) and eliminate resonance terms by equating to zero the coefficients of $\cos(\xi)$ and $\sin(\xi)$. Doing so yields the "slow flow" equations on coefficients A and B. The slow flow equations on A and B both contain 588 terms, so we omit printing them here. However, the equations are all of the form

$$\frac{dA}{d\eta} = Y_{111}A^3 + Y_{112}A^2B + Y_{121}AB^2 + Y_{122}B^3 + Y_{101}A + Y_{102}B \tag{3.31}$$

$$\frac{dB}{d\eta} = Y_{211}A^3 + Y_{212}A^2B + Y_{221}AB^2 + Y_{222}B^3 + Y_{201}A + Y_{202}B \tag{3.32}$$

where Y_{ijk} are all constant functions depending on the parameters c, P and T_{cr}, ω_{cr}.

In order to solve the system of equations (3.31), (3.32), we transform the problem to polar coordinates, setting:

$$A(\eta) = R(\eta)\cos(\theta(\eta))$$

$$B(\eta) = R(\eta)\sin(\theta(\eta))$$

This results in a slow flow equation of the form

$$\frac{dR}{d\eta} = \Gamma_1 R^3 - \Gamma_2 \mu_2 R \tag{3.33}$$

$$\frac{d\theta}{d\eta} = \Gamma_3 R^2 + \Gamma_4 \mu_2 + k_2 \tag{3.34}$$

where the Γ_i are known constants.

Equilibria of the slow flow equations correspond to limit cycles in the full system. The nontrivial equilibrium point for eq. (3.33) will give a prediction for the amplitude of the corresponding limit cycle depending on μ_2. We choose k_2 such that when eq. (3.33) is at equilibrium for some R_{eq}, then $\frac{d\theta}{d\eta} = 0$ in eq. (3.34). Table 3.3 provides results of the perturbation method for the given T_α parameter values.

Finally, we note that for the Hopf bifurcations in Table 3.3, Γ_1 and Γ_2 are both positive. This shows that limit cycles occur for $\mu_2 > 0$. Furthermore, it confirms our earlier analysis suggesting that Hopf bifurcations which occur with time delay T_α are supercritical because linearization about the equilibrium radius R_{eq} yields that the equilibrium point of the slow flow (corresponding to the limit cycle that is the in-phase mode) is stable.

A comparison of these results with numerical continuation is provided in Figure 3.6 below. The continuation curves were generated using `DDE-BIFTOOL`.

Table 3.3: Results of the Two-Variable Expansion method for the parameter values $P = 10$, $\gamma = \frac{4}{3}$ on eq. (3.5) where $\Delta = \epsilon^2\mu_2 = T - T_{\rm cr}$.

n	T_{cr}	$R_{eq}/\sqrt{\Delta}$	k_2/Δ
0	0.9672	1.4523	-1.4506
1	4.0332	.81566	-.45758
2	7.0991	.62844	-.27136
3	10.165	.52993	-.19314
4	13.231	.46676	-.14984
5	16.297	.42187	-.12240
6	19.362	.38784	-.10346

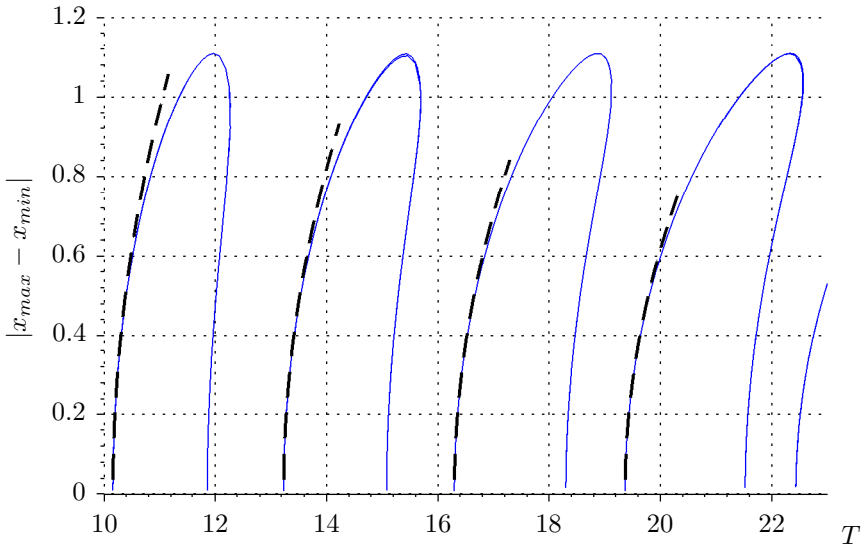

Figure 3.6: Continuation and perturbation methods compared for a series of Hopf points. Dashed lines correspond to perturbation results, whereas solid lines correspond to continuation.

3.4 Stability of the In-Phase Manifold

While the above analysis has ascertained that, for the Hopf bifurcations associated with time delay T_α, the in-phase mode is stable, the question remains for

the original equations (3.1), (3.2) whether the motion is stable. That is, we have so far analyzed the dynamics only when restricted to the initial conditions $a = b$, $\dot{a} = \dot{b}$, and we have ascertained the local stability of the in-phase mode restricted to this space. However, if more general initial conditions are considered, will the periodic motions born out of the supercritical Hopf bifurcations be stable?

To answer this question, we will no longer restrict our analysis to the in-phase manifold equation (3.5) and instead will investigate the full system (3.1), (3.2). We will again recognize that these equations exhibit the equilibrium solution $a_e = b_e = 1$, so we will look at deviations from that motion. We set $a = a_e + \epsilon x, b = b_e + \epsilon y$, solve for $\ddot{x}$ and take the Taylor series approximation for the system for small ϵ. After dividing both sides by a shared factor of ϵ, this will transform the system (3.1), (3.2) into:

$$\begin{aligned} c\ddot{x} + 4\dot{x} + 4cx + P\dot{y}(t-T) = \frac{1}{2c}(((28x^2 - 3\dot{x}^2)c^2 + c(24\dot{x} + 2P\dot{y}(t-T))x \\ - 8\dot{x}^2 - 2P\dot{y}(t-T)\dot{x})\epsilon) \\ - \frac{1}{2c^2}(c^3(68x^3 - 3\dot{x}^2x) + c^2((64\dot{x}x^2 + 2P\dot{y}(t-T))x^2 + 2\dot{x}^3) \\ + c(-24\dot{x}^2 - 2P\dot{y}(t-T)\dot{x})x + 8\dot{x}^3 + 2P\dot{y}(t-T)\dot{x}^2)\epsilon^2 + O(\epsilon^3) \end{aligned} \tag{3.35}$$

$$\begin{aligned} c\ddot{y} + 4\dot{y} + 4cy + P\dot{x}(t-T) = \frac{1}{2c}(((28y^2 - 3\dot{y}^2)c^2 + c(24\dot{y} + 2P\dot{x}(t-T))y \\ - 8\dot{y}^2 - 2P\dot{x}(t-T)\dot{y})\epsilon) \\ - \frac{1}{2c^2}(c^3(68y^3 - 3\dot{y}^2y) + c^2((64\dot{y}y^2 + 2P\dot{x}(t-T))y^2 + 2\dot{y}^3) \\ + c(-24\dot{y}^2 - 2P\dot{x}(t-T)\dot{y})y + 8\dot{y}^3 + 2P\dot{x}(t-T)\dot{y}^2)\epsilon^2 + O(\epsilon^3) \end{aligned} \tag{3.36}$$

Note that we have already substituted $\gamma = \frac{4}{3}$ from eq. (3.9). In the nomenclature of the above formulation, eqs. (3.1), (3.2) support a Hopf bifurcation in the

in-phase manifold $x = y = f(t)$ (the periodic motion):

$$\begin{aligned} c\ddot{f} + 4\dot{f} + 4cf + P\dot{f}(t-T) = \frac{1}{2c}(((28f^2 - 3\dot{f}^2)c^2 + c(24\dot{f} + 2P\dot{f}(t-T))f \\ - 8\dot{f}^2 - 2P\dot{f}(t-T)\dot{f})\epsilon) \\ - \frac{1}{2c^2}(c^3(68f^3 - 3\dot{f}^2 f) + c^2((64\dot{f}f^2 + 2P\dot{f}(t-T))f^2 + 2\dot{f}^3) \\ + c(-24\dot{f}^2 - 2P\dot{f}(t-T)\dot{f})f + 8\dot{f}^3 + 2P\dot{f}(t-T)\dot{f}^2)\epsilon^2 + O(\epsilon^3) \quad (3.37) \end{aligned}$$

We have found the approximate solution of eq. (3.37) for $c = 94$, $P = 10$ and $T = T_{\text{cr}} + \Delta$ to be:

$$f(t) = R_{eq}\cos((\omega_{\text{cr}} + \epsilon^2 k_2)t) \quad (3.38)$$

where R_{eq}, k_2 are calculated in the previous section for delays T_{cr} corresponding to supercritical Hopfs, see Table 3.3. The goal is to determine the stability of the motion $f(t)$ in eq. (3.38). To do this, one may analyze the linear variational equations of eqs. (3.35), (3.36). Setting $x = \delta x + f, y = \delta y + f$ and expanding for small $\delta x, \delta y$ results in the linear variational equations shown in eqs. (3.39), (3.40). Note that here, the notation $\dot{x}_{\text{d}} = \dot{x}(t - T_{\text{cr}})$ and the same for y is used.

$$
\begin{aligned}
&c\delta\ddot{x}+4c\delta\dot{x}+4\delta x+P\delta\dot{y}_{\mathrm{d}}= \\
&\quad -\frac{1}{c}((3\dot{f}\delta\dot{x}-28f\delta x)c^2+(-12f\delta\dot{x}+(-P\dot{f}_{\mathrm{d}}-12\dot{f})\delta x-fP\delta\dot{y}_{\mathrm{d}})c \\
&\quad +(P\dot{f}_{\mathrm{d}}+8\dot{f})\delta\dot{x}+P\dot{f}\delta\dot{y}_{\mathrm{d}})\epsilon \\
&\quad +(((6f\dot{f}\delta\dot{x}+(3\dot{f}^2-204f^2)\delta x)c^3+((-6\dot{f}^2-64f^2)\delta\dot{x} \\
&\quad +(-4Pf\dot{f}_{\mathrm{d}}-128f\dot{f})\delta x-2Pf^2\delta\dot{y}_{\mathrm{d}})c^2+((2Pf\dot{f}_{\mathrm{d}}+48f\dot{f})\delta\dot{x} \\
&\quad +(2P\dot{f}_{\mathrm{d}}\dot{f}+24\dot{f}^2)\delta x+2Pf\dot{f}\delta\dot{y}_{\mathrm{d}})c+(-4P\dot{f}_{\mathrm{d}}\dot{f}-24\dot{f}^2)\delta\dot{x}-2P\dot{f}^2\delta\dot{y}_{\mathrm{d}})\epsilon^2)/(2c^2) \\
&\quad +O(\epsilon^3)
\end{aligned}
\tag{3.39}
$$

$$
\begin{aligned}
&c\delta\ddot{y}+4c\delta\dot{y}+4\delta y+P\delta\dot{x}_{\mathrm{d}}= \\
&\quad -\frac{1}{c}((3\dot{f}\delta\dot{y}-28f\delta y)c^2+(-12f\delta\dot{y}+(-P\dot{f}_{\mathrm{d}}-12\dot{f})\delta y-fP\delta\dot{x}_{\mathrm{d}})c \\
&\quad +(P\dot{f}_{\mathrm{d}}+8\dot{f})\delta\dot{y}+P\dot{f}\delta\dot{x}_{\mathrm{d}})\epsilon \\
&\quad +(((6f\dot{f}\delta\dot{y}+(3\dot{f}^2-204f^2)\delta y)c^3+((-6\dot{f}^2-64f^2)\delta\dot{y} \\
&\quad +(-4Pf\dot{f}_{\mathrm{d}}-128f\dot{f})\delta y-2Pf^2\delta\dot{x}_{\mathrm{d}})c^2+((2Pf\dot{f}_{\mathrm{d}}+48f\dot{f})\delta\dot{y} \\
&\quad +(2P\dot{f}_{\mathrm{d}}\dot{f}+24\dot{f}^2)\delta y+2Pf\dot{f}\delta\dot{x}_{\mathrm{d}})c+(-4P\dot{f}_{\mathrm{d}}\dot{f}-24\dot{f}^2)\delta\dot{y}-2P\dot{f}^2\delta\dot{x}_{\mathrm{d}})\epsilon^2)/(2c^2) \\
&\quad +O(\epsilon^3)
\end{aligned}
\tag{3.40}
$$

To analyze eqs. (3.39), (3.40), we set $u = \delta x - \delta y$ and $v = \delta x + \delta y$ in order to transform the problem into "in-phase" and "out-of-phase" coordinates. We then add and subtract eqs. (3.39), (3.40) to and from one another respectively to obtain

$$
\begin{aligned}
&c\ddot{u}+4\dot{u}+4uc-P\dot{u}_{\mathrm{d}}= \\
&\quad\frac{(\dot{f}-cf)P\dot{u}_{\mathrm{d}}+(-\dot{f}_{\mathrm{d}}P+(-3c^2-8)\dot{f}+12cf)\dot{u}+(c\dot{f}_{\mathrm{d}}P+12c\dot{f}+28c^2f)u}{c}\epsilon \\
&\quad+(((2\dot{f}^2-2cf\dot{f}+2c^2f^2)P\dot{u}_{\mathrm{d}}+((-4\dot{f}+2cf)\dot{f}_{\mathrm{d}}P+(-6c^2-24)\dot{f}^2 \\
&\quad+(6c^3+48c)f\dot{f}-64c^2f^2)\dot{u}+((2c\dot{f}-4c^2f)\dot{f}_{\mathrm{d}}P+(3c^3+24c)\dot{f}^2-128c^2f\dot{f} \\
&\quad-204c^3f^2)u)\epsilon^2)/(2c^2)+O(\epsilon^3) \qquad (3.41)
\end{aligned}
$$

$$
\begin{aligned}
&c\ddot{v}+4\dot{v}+4vc+P\dot{v}_{\mathrm{d}}= \\
&\quad-\frac{(\dot{f}-cf)P\dot{v}_{\mathrm{d}}+(\dot{f}_{\mathrm{d}}P+(3c^2+8)\dot{f}-12cf)\dot{v}+(-c\dot{f}_{\mathrm{d}}P-12c\dot{f}-28c^2f)v}{c}\epsilon \\
&\quad-(((2\dot{f}^2-2cf\dot{f}+2c^2f^2)P\dot{v}_{\mathrm{d}}+((4\dot{f}-2cf)\dot{f}_{\mathrm{d}}P+(6c^2+24)\dot{f}^2 \\
&\quad+(-6c^3-48c)f\dot{f}+64c^2f^2)\dot{v}+((-2c\dot{f}+4c^2f)\dot{f}_{\mathrm{d}}P+(-3c^3-24c)\dot{f}^2+128c^2f\dot{f} \\
&\quad+204c^3f^2)v)\epsilon^2)/(2c^2)+O(\epsilon^3) \qquad (3.42)
\end{aligned}
$$

Note that eq. (3.42) is the variational equation of eq. (3.37). Because of this, it is seen that v determines the stability of the motion $x = y = f(t)$ *in* the in-phase manifold, while u determines the stability *of* the in-phase manifold. Since eq. (3.42) is a linear delay-differential equation, its solution space is spanned by an infinite number of linearly independent solutions. One of these solutions is $v = \frac{df}{dt}$, as may be seen by differentiating eq. (3.37) and comparing with eq. (3.42). The solution is periodic since $f(t)$ is periodic. All other solutions of eq. (3.42) are expected to be asymptotically stable for small ϵ, since as proven in the previous section, $f(t)$ is a limit cycle born in a supercritical Hopf bifurcation. Therefore, the stability of the in-phase mode $x = y = f(t)$ is determined solely by eq. (3.41).

It is notable that a basic difference between eqs. (3.41) and (3.42) is that when $\epsilon = 0$, eq. (3.42) exhibits a periodic solution (due to the Hopf bifurcation), while eq. (3.41) does not. Thus, at $\epsilon = 0$, eq. (3.42) is structurally unstable, whereas eq.

(3.41) is structurally stable. Therefore, for small values of ϵ, the stability of eq. (3.41) is the same as it is for $\epsilon = 0$. The stability of eq. (3.41) (and of the in-phase mode $x = y = f(t)$) is then determined by the behavior of the $\epsilon = 0$ version of eq. (3.41):

$$c\ddot{u} + 4\dot{u} + 4cu - P\dot{u}(t - T_{\text{cr}}) = 0 \tag{3.43}$$

To solve eq. (3.43), set $u = \exp(\lambda t)$ and obtain the characteristic equation

$$c\lambda^2 + 4\lambda + 4c\lambda - P\exp(-\lambda T_{\text{cr}}) = 0 \tag{3.44}$$

Writing $\lambda = a + ib$ and equating imaginary and real parts yields:

$$0 = P\exp(-aT_{\text{cr}})\sin(bT_{\text{cr}}) + 4b + 2abc \tag{3.45}$$

$$0 = P\exp(-aT_{\text{cr}})\cos(bT_{\text{cr}}) - 4a + c(b^2 - a^2 - 4) \tag{3.46}$$

For stability, all roots to eqs. (3.45), (3.46) must have $a < 0$. For instability, there must be at least one root for which $a > 0$.

Figure 3.7 shows plots of the implicit functions in eqs. (3.45), (3.46), where intersections of the curves designate solutions to the system of simultaneous equations. Inspection shows that there are no roots for which $a > 0$, showing that the in-phase mode is stable. These plots are only shown for the first few values of delay for which their is a supercritical Hopf bifurcation.

This conclusion is supported by numerical integration using the MATLAB toolbox `dde23`, for which we show a characteristic time integration in Figure

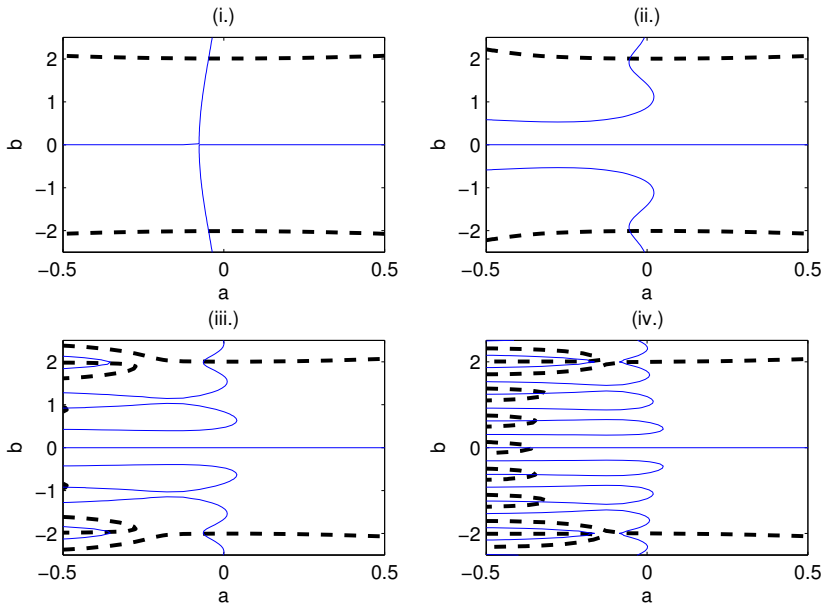

Figure 3.7: Plot of the curves in eqs. (3.45), (3.46) for (i.) $T_{\rm cr} = 0.96734$, (ii.) $T_{\rm cr} = 4.03324$, (iii.) $T_{\rm cr} = 7.09919$, and (iv.) $T_{\rm cr} = 10.165$. Solid lines are plots of eq. (3.45), dashed lines are plots of eq. (3.46).

3.8. The time integration features an arbitrary choice of initial conditions off the in-phase manifold, and it is witnessed that the solution approaches the in-phase mode.

3.5 Conclusion

This work has investigated the stability of periodic motions that arise from a differential-delay equation associated with the coupled dynamics of two oscillating bubbles. The delayed dynamics arise as a result of the finite speed of sound in the surrounding fluid, leading to a non-negligible propagation time for waves created by one bubble to reach the other.

The main focus of study for the problem is the invariant manifold on which

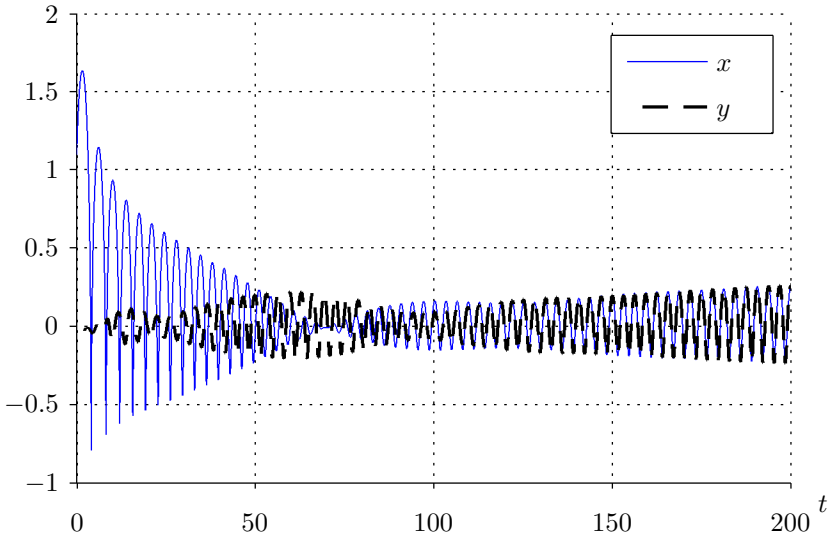

Figure 3.8: Time series integration for arbitrary initial conditions (here, $(x_0, \dot{x}_0, y_0, \dot{y}_0) = (1.1, 0, 0.8, 0)$) for the bubble equation just past a supercritical Hopf bifurcation with $T = 4.2$.

the bubble dynamics are identical, which is termed the "in-phase manifold." The study investigated the dynamics of the in-phase manifold, particularly around the equilibrium radius of the bubble. It is shown that this equilibrium point undergoes a Hopf bifurcation in response to a change in delay T giving rise to limit cycles. There are two sequences of Hopf bifurcations that occur at distinct intervals, with one shown to be always supercritical while the other subcritical. The supercritical Hopf bifurcations are further characterized by use of the two-variable expansion method, which provides a formal prediction for amplitude and frequency of oscillations based on the delay parameter.

With the stability picture of the in-phase mode on the in-phase manifold established, the stability of the manifold itself is then established. Through the use of linear variational equations for the periodic motion born in the Hopf bifurcation, it is shown that for arbitrary initial conditions near the in-phase

mode, all motions will approach the in-phase manifold. Therefore, the analysis of the in-phase mode is complete; it is determined that, when it exists, the in-phase mode is stable.

CHAPTER 4

ANALYSIS OF THE HOPF-HOPF BIFURCATION

4.1 Introduction

Delay in dynamical systems is exhibited whenever the system's behavior is dependent at least in part on its history. Many technological and biological systems are known to exhibit such behavior; coupled laser systems, high-speed milling, population dynamics and gene expression are some examples of delayed systems. This work analyzes a simple differential delay equation that is motivated by a system of two microbubbles coupled by acoustic forcing, previously studied by Heckman *et al.* [6, 3, 1, 2]. The propagation time of sound in the fluid gives rise to a time delay between the two bubbles. The system under study has the same linearization as the equations previously studied, and like them it supports a double Hopf or Hopf-Hopf bifurcation[18] for special values of the system parameters. In order to study the dynamics associated with this type of bifurcation, we replace the nonlinear terms in the original microbubble model with a simpler nonlinearity, namely a cubic term:

$$\kappa\ddot{x} + 4\dot{x} + 4\kappa x + 10\dot{x}_d = \epsilon x^3. \tag{4.1}$$

where $x_d = x(t - T)$.

The case of a typical Hopf bifurcation (not a double Hopf) in a system of DDEs has been shown to be treatable by both Lindstedt's method and center manifold analysis [33, 32]. The present paper investigates the use of these methods on a DDE which exhibits a double Hopf. This type of bifurcation occurs

when two pairs of complex conjugate roots of the characteristic equation simultaneously cross the imaginary axis in the complex plane. These considerations are dependent only on the linear part of the DDE. If nonlinear terms are present, multiple periodic limit cycles may occur, and in addition to these, quasiperiodic motions may occur, where the quasiperiodicity is due to the two frequencies associated with the pair of imaginary roots in the double Hopf.

Other researchers have investigated Hopf-Hopf bifurcations, as follows. Xu *et al.*[40] developed a method called the perturbation-incremental scheme (PIS) and used it to study bifurcation sets in (among other systems) the van der Pol-Duffing oscillator. They show a robust method for approximating complex behavior both quantitatively and qualitatively in the presence of strong nonlinearities. A similar oscillator system was also studied by Ma *et al.*[27], who applied a center manifold reduction and found quasiperiodic solutions born out of a Neimark-Sacker bifurcation. Such quasiperiodicity in differential-delay equations is well established and has also been studied by e.g. Yu *et al.*[42, 9] by investigating Poincaré maps. They also show that chaos naturally evolves via the breakup of tori in the phase space. A study of a general differential delay equation near a nonresonant Hopf-Hopf bifurcation was conducted by Buono *et al.*[8], who also gave a description of the dynamics of a differential delay equation by means of ordinary differential equations on center manifolds.

In this work we analyze a model problem using both Lindstedt's method and center manifold reduction, and we compare results with those obtained by numerical methods, i.e. continuation software.

4.2 Lindstedt's Method

A Hopf-Hopf bifurcation is characterized by a pair of characteristic roots crossing the imaginary axis at the same parameter value. In order to obtain approximations for the resulting limit cycles, we will first use a version of Lindstedt's method which perturbs off of simple harmonic oscillators. Then the unperturbed solution will have the form:

$$x_0 = A\cos\tau + B\sin\tau$$

where

$$\tau = \omega_i t, \qquad i = 1, 2$$

where $i\omega_1$ and $i\omega_2$ are the associated imaginary characteristic roots.

The example system under analysis is motivated by the Rayleigh-Plesset Equation with Delay Coupling (RPE), as studied by Heckman *et al.* [6, 3]. The equation of motion for a spherical bubble contains quadratic nonlinearities and multiple parameters quantifying the fluids' mechanical properties; eq. (4.1), the object of study in this work, is designed to capture the salient dynamical properties of the RPE while simplifying analysis.

Eq. (4.1) has the same linearization as the RPE, with a cubic nonlinear term added to it. This system has an equilibrium point at $x = 0$ that will correspond to the local behavior of the RPE's equilibrium point as a result.

For $\epsilon = 0$, eq. (4.1) exhibits a Hopf-Hopf bifurcation with approximate parameters[1]:

$$\kappa = 6.8916, \quad T = T^* = 2.9811,$$

$$\omega_1 = \omega_a = 1.4427, \quad \omega_2 = \omega_b = 2.7726$$

where ω_a, ω_b are values of ω_i at the Hopf-Hopf. As usual in Lindstedt's method we replace t by τ as independent variable, giving

$$\kappa\omega^2 x'' + 4\omega x' + 4\kappa x + 10\omega x'_d = \epsilon x^3$$

where ω stands for either ω_1 or ω_2. Next we expand x in a power series in ϵ:

$$x = x_0 + \epsilon x_1 + \cdots$$

and we also expand ω:

$$\omega = \omega^* + \epsilon p + \cdots$$

We expect the amplitude of oscillation and the frequency shift p to change in response to a detuning of delay T off of the Hopf-Hopf value T^*:

$$T = T^* + \epsilon\Delta$$

For the delay term we have:

$$x_d = x_{0_d} + \epsilon x_{1_d} + \cdots$$

where

$$\begin{aligned} x_{0_d}(\tau) &= x_0(\tau - \omega T) \\ &= x_0(\tau - (\omega^* + \epsilon p)(T^* + \epsilon\Delta)) \\ &= x_0(\tau - \omega^* T^*) - \epsilon(pT^* + \omega^*\Delta)x_0'(\tau - \omega^* T^*) + \cdots \end{aligned}$$

Differentiating,

$$x_d' = x_0'(\tau - \omega^* T^*) - \epsilon(pT^* + \omega^*\Delta)x_0''(\tau - \omega^* T^*) + \epsilon x_1'(\tau - \omega^* T^*) + \cdots$$

We introduce the following abbreviation for a delay argument:

$$f(*) = f(\tau - \omega^* T^*)$$

Then

$$x_d' = x_0'(*) - \epsilon(pT^* + \omega^*\Delta)x_0''(*) + \epsilon x_1'(*) + \cdots$$

Next we substitute the foregoing expressions into the eq. (4.1) which gives

$$\begin{aligned} &\kappa(\omega^* + \epsilon p)^2(x_0'' + \epsilon x_1'') + 4(\omega^* + \epsilon p)(x_0' + \epsilon x_1') + 4\kappa(x_0 + \epsilon x_1) \\ &+ 10(\omega^* + \epsilon p)(x_0'(*) - \epsilon(pT^* + \omega^*\Delta)x_0''(*) + \epsilon x_1'(*)) = \epsilon x_0^3 \end{aligned}$$

and collect terms, giving:

$$\epsilon^0 : \quad Lx_0 = 0$$

where

$$Lf(\tau) = \kappa\omega^{*2} f'' + 4\omega^* f' + 4\kappa f + 10\omega^* f'(*)$$

$$\epsilon^1 : \quad Lx_1 = -G(x_0)$$

and

$$G(x_0) = 2\kappa\omega^* p x_0'' + 4p x_0' + 10p x_0'(*) - 10\omega^*(pT^* + \omega^*\Delta)x_0''(*) - x_0^3$$

Next we solve $Lx_0 = 0$ for the delayed quantity $x_0'(*)$ with the idea of replacing it in G by non-delayed quantities. We find

$$x_0'(*) = -\frac{1}{10\omega^*}\left\{\kappa\omega^{*2} x_0'' + 4\omega^* x_0' + 4\kappa x_0\right\}$$

Since G contains the quantity $x_0''(*)$, we differentiate the foregoing formula to obtain:

$$x_0''(*) = -\frac{1}{10\omega^*}\left\{\kappa\omega^{*2} x_0''' + 4\omega^* x_0'' + 4\kappa x_0'\right\}$$

We obtain

$$
\begin{aligned}
G(x_0) &= 2\kappa\omega^* p x_0'' + 4p x_0' - \frac{p}{\omega^*}(\kappa\omega^{*2} x_0'' + 4\omega^* x_0' + 4\kappa x_0) \\
&\quad + (pT^* + \omega^*\Delta)(\kappa\omega^{*2} x_0''' + 4\omega^* x_0'' + 4\kappa x_0') - x_0^3 \\
&= \kappa\omega^* p x_0'' - \frac{4\kappa p}{\omega^*} x_0 + (pT^* + \omega^*\Delta)(\kappa\omega^{*2} x_0''' + 4\omega^* x_0'' \\
&\quad + 4\kappa x_0') - x_0^3
\end{aligned}
$$

Now we take $x_0 = A\cos\tau$ and require the coefficients of $\cos\tau$ and $\sin\tau$ in G to vanish for no secular terms. We obtain:

$$
\begin{aligned}
\cos\tau: &\quad A(-\kappa\omega^* p - \frac{4\kappa p}{\omega^*} + (pT^* + \omega^*\Delta)(-4\omega^*) - \frac{3}{4}A^2) = 0 \\
\sin\tau: &\quad A(pT^* + \omega^*\Delta)(\kappa\omega^{*2} - 4\kappa) = 0
\end{aligned}
$$

The second of these gives

$$
p = -\frac{\omega^*}{T^*}\Delta
$$

whereupon the first gives

$$
A^2 = -\frac{4}{3\omega^*}\kappa p(\omega^{*2} + 4)
$$

which may be rewritten using the foregoing expression for p:

$$
A^2 = \frac{4}{3T^*}\kappa(\omega^{*2} + 4)\Delta
$$

Using $\kappa = 6.8916$ and $T^* = 2.9811$, we obtain:

$$A^2 = 3.0823(\omega^{*2} + 4)\Delta$$

This gives

$$A = 4.3295\sqrt{\Delta} \qquad \text{for} \qquad \omega_a = 1.4427$$

and

$$A = 6.0020\sqrt{\Delta} \qquad \text{for} \qquad \omega_b = 2.7726$$

4.3 Center Manifold Reduction

We now approach the same problem via a center manifold reduction method, wherein the critical dynamics of eq. (4.1) at the Hopf-Hopf bifurcation are analyzed by seeking a four-dimensional center manifold description corresponding to the codimension-2 Hopf-Hopf.

In order to put Eq. (4.1) into a form amenable to treatment by functional analysis, we draw on the method used by Kalmár-Nagy *et al.* [21] and Rand [33, 32]. The operator differential equation for this system will now be developed. Eq. (4.1) may be written in the form:

$$\dot{\mathbf{x}}(t) = \mathbf{L}(\kappa)\mathbf{x}(t) + \mathbf{R}(\kappa)\mathbf{x}(t-\tau) + \mathbf{f}(\mathbf{x}(t), \mathbf{x}(t-\tau), \kappa)$$

where

$$\mathbf{x}(t) = \begin{pmatrix} x(t) \\ \dot{x}(t) \end{pmatrix} = \begin{pmatrix} x_1 \\ x_2 \end{pmatrix}$$

$$\mathbf{L}(\kappa) = \begin{pmatrix} 0 & 1 \\ -4 & -4/\kappa \end{pmatrix}, \mathbf{R}(\kappa) = \begin{pmatrix} 0 & 0 \\ 0 & -10/\kappa \end{pmatrix}$$

and

$$\mathbf{f}(\mathbf{x}(t), \mathbf{x}(t-\tau), \kappa) = \begin{pmatrix} 0 \\ (\epsilon/\kappa)x_1^3 \end{pmatrix}$$

Note that the initial conditions to a differential delay equation consists of a function defined on $-\tau \leq t \leq 0$. As t increases from zero, the initial function on $[-\tau, 0]$ evolves to one on $[-\tau + t, t]$. This implies the flow is determined by a function whose initial conditions are shifting. In order to make the differential delay equation problem tenable to analysis, it is advantageous to recast it in the context of functional analysis.

To accomplish this, we consider a function space of continuously differential functions on $[-\tau, 0]$. The time variable t specifies which function is being considered, namely the one corresponding to the interval $[-\tau + t, t]$. The *phase* variable θ specifies a point in the interval $[-\tau, 0]$.

Now, the variable $\mathbf{x}(t + \theta)$ represents the point in the function space which has evolved from the initial condition function $\mathbf{x}(\theta)$ at time t. From the point of view of the function space, t is now a parameter, whereas θ is the independent variable. To emphasize this new definition, we write

$$\mathbf{x}_t(\theta) = \mathbf{x}(t+\theta), \quad \theta \in [-\tau, 0].$$

The delay differential equation may therefore be expressed as

$$\dot{\mathbf{x}}_t = \mathcal{A}\mathbf{x}_t + \mathcal{F}(\mathbf{x}_t), \tag{4.2}$$

If κ^* is the critical value of the bifurcation parameter, and noting that $\frac{\partial \mathbf{x}_t(\theta)}{\partial t} = \frac{\partial \mathbf{x}_t(\theta)}{\partial \theta}$ (which follows from $\mathbf{x}_t(\theta) = \mathbf{x}(t+\theta)$), then when $\kappa = \kappa^*$ the operator differential equation has components

$$\mathcal{A}\mathbf{u}(\theta) = \begin{cases} \frac{d}{d\theta}\mathbf{u}(\theta) & \theta \in [-\tau, 0) \\ \mathbf{L}\mathbf{u}(0) + \mathbf{R}\mathbf{u}(-\tau) & \theta = 0 \end{cases} \tag{4.3}$$

and

$$\mathcal{F}(\mathbf{u}(\theta)) = \begin{cases} \mathbf{0} & \theta \in [-\tau, 0) \\ \begin{pmatrix} 0 \\ (\epsilon/\kappa)\, u_1(0)^3 \end{pmatrix} & \theta = 0 \end{cases} \tag{4.4}$$

The linear mapping of the original equation is given by

$$\mathcal{L}(\phi(\theta)) = \mathbf{L}(\kappa)\phi(0) + \mathbf{R}(\kappa)\phi(-\tau)$$

where $\mathbf{x}(t) = \phi(t)$ for $t \in [-\tau, 0]$, $\mathbf{F} : \mathcal{H} \to \mathbb{R}^2$ is a nonlinear functional defined by

$$\mathbf{F}(\phi(\theta)) = \mathbf{f}(\phi(0), \phi(-\tau)),$$

and where $\mathcal{H} = C([-\tau, 0], \mathbb{R}^2)$ is the Banach space of continuously differentiable functions $\mathbf{u} = \begin{pmatrix} u_1 \\ u_2 \end{pmatrix}$ from $[-\tau, 0]$ into $\mathbb{R}^2$.

Eqs. (4.3) and (4.4) are representations of eq. (4.1) in "canonical form." They contain the corresponding linear and nonlinear parts of eq. (4.1) as the boundary conditions to the full evolution equation (4.2).

A stability analysis of eq. (4.3) alone provides insight into the asymptotic stability of the original equations. In the case when eq. (4.3) has neutral stability (i.e. has eigenvalues with real part zero), analysis of eq. (4.4) is necessary. The purpose of the center manifold reduction is to project the dynamics of the infinite-dimensional singular case onto a low-dimensional subspace on which the dynamics are more analytically tractable.

At a bifurcation, the critical eigenvalues of the operator $\mathcal{A}$ coincide with the critical roots of the characteristic equation. In this system, the target of analysis is a Hopf-Hopf bifurcation, a codimension-2 bifurcation that has a four-dimensional center manifold [17]. Consequently, there will be two pairs of critical eigenvalues $\pm i\omega_a$ and $\pm i\omega_b$ with real part zero. Each eigenvalue has an eigenspace spanned by the real and imaginary parts of its corresponding complex eigenfunction. These eigenfunctions are denoted $\mathbf{s}_a(\theta), \mathbf{s}_b(\theta) \in \mathcal{H}$.

The eigenfunctions satisfy

$$\mathcal{A}\mathbf{s}_a(\theta) = i\omega_a \mathbf{s}_a(\theta)$$

$$\mathcal{A}\mathbf{s}_b(\theta) = i\omega_b \mathbf{s}_b(\theta);$$

or equivalently,

$$\mathcal{A}(\mathbf{s}_{a1}(\theta) + i\mathbf{s}_{a2}(\theta)) = i\omega_a(\mathbf{s}_{a1}(\theta) + i\mathbf{s}_{a2}(\theta)) \tag{4.5}$$

$$\mathcal{A}(\mathbf{s}_{b1}(\theta) + i\mathbf{s}_{b2}(\theta)) = i\omega_b(\mathbf{s}_{b1}(\theta) + i\mathbf{s}_{b2}(\theta)) \tag{4.6}$$

Equating real and imaginary parts in eq. (4.5) and eq. (4.6) gives

$$\mathcal{A}\mathbf{s}_{a1}(\theta) = -\omega_a\mathbf{s}_{a2}(\theta) \tag{4.7}$$

$$\mathcal{A}\mathbf{s}_{a2}(\theta) = \omega_a\mathbf{s}_{a1}(\theta) \tag{4.8}$$

$$\mathcal{A}\mathbf{s}_{b1}(\theta) = -\omega_b\mathbf{s}_{b2}(\theta) \tag{4.9}$$

$$\mathcal{A}\mathbf{s}_{b2}(\theta) = \omega_b\mathbf{s}_{b1}(\theta). \tag{4.10}$$

Applying the definition of $\mathcal{A}$ to eqs. (4.7)-(4.10) produces the differential equations

$$\frac{d}{d\theta}\mathbf{s}_{a1}(\theta) = -\omega_a\mathbf{s}_{a2}(\theta) \tag{4.11}$$

$$\frac{d}{d\theta}\mathbf{s}_{a2}(\theta) = \omega_a\mathbf{s}_{a1}(\theta) \tag{4.12}$$

$$\frac{d}{d\theta}\mathbf{s}_{b1}(\theta) = -\omega_b\mathbf{s}_{b2}(\theta) \tag{4.13}$$

$$\frac{d}{d\theta}\mathbf{s}_{b1}(\theta) = \omega_b\mathbf{s}_{b1}(\theta) \tag{4.14}$$

with boundary conditions

$$\mathbf{L}\mathbf{s}_{a1}(0) + \mathbf{R}\mathbf{s}_{a1}(-\tau) = -\omega_a \mathbf{s}_{a2}(0) \tag{4.15}$$

$$\mathbf{L}\mathbf{s}_{a2}(0) + \mathbf{R}\mathbf{s}_{a2}(-\tau) = \omega_a \mathbf{s}_{a1}(0) \tag{4.16}$$

$$\mathbf{L}\mathbf{s}_{b1}(0) + \mathbf{R}\mathbf{s}_{b1}(-\tau) = -\omega_b \mathbf{s}_{b2}(0) \tag{4.17}$$

$$\mathbf{L}\mathbf{s}_{b2}(0) + \mathbf{R}\mathbf{s}_{b2}(-\tau) = \omega_b \mathbf{s}_{b1}(0) \tag{4.18}$$

The general solution to the differential equations (4.11)-(4.14) is:

$$\mathbf{s}_{a1}(\theta) = \cos(\omega_a\theta)\mathbf{c}_{a1} - \sin(\omega_a\theta)\mathbf{c}_{a2}$$

$$\mathbf{s}_{a2}(\theta) = \sin(\omega_a\theta)\mathbf{c}_{a1} + \cos(\omega_a\theta)\mathbf{c}_{a2}$$

$$\mathbf{s}_{b1}(\theta) = \cos(\omega_b\theta)\mathbf{c}_{b1} - \sin(\omega_b\theta)\mathbf{c}_{b2}$$

$$\mathbf{s}_{b2}(\theta) = \sin(\omega_b\theta)\mathbf{c}_{b2} + \cos(\omega_b\theta)\mathbf{c}_{b2}$$

where $\mathbf{c}_{\alpha i} = \begin{pmatrix} c_{\alpha i1} \\ c_{\alpha i2} \end{pmatrix}$. This results in eight unknowns which may be solved by applying the boundary conditions (4.15)-(4.18). However, since we are searching for a nontrivial solution to these equations, they must be linearly dependent. We set the value of four of the unknowns to simplify the final result:

$$c_{a11} = 1, \quad c_{a21} = 0, \quad c_{b11} = 1, \quad c_{b21} = 0. \tag{4.19}$$

This allows eqs. (4.15)-(4.18) to be solved uniquely, yielding

$$\mathbf{c}_{a1} = \begin{pmatrix} 1 \\ 0 \end{pmatrix}, \quad \mathbf{c}_{a2} = \begin{pmatrix} 0 \\ \omega_a \end{pmatrix}, \quad \mathbf{c}_{b1} = \begin{pmatrix} 1 \\ 0 \end{pmatrix}, \quad \mathbf{c}_{b2} = \begin{pmatrix} 0 \\ \omega_b \end{pmatrix}.$$

Next, the vectors that span the dual space $\mathcal{H}^*$ must be calculated. The boundary value problem associated with this case has the same differential equations (4.11)-(4.14) except on $\mathbf{n}_{\alpha i}$ rather than on $\mathbf{s}_{\alpha i}$; in place of boundary conditions (4.15)-(4.18), there are boundary conditions

$$\mathbf{L}^T\mathbf{n}_{a1}(0) + \mathbf{R}^T\mathbf{n}_{a1}(\tau) = \omega_a\mathbf{n}_{a2}(0) \tag{4.20}$$

$$\mathbf{L}^T\mathbf{n}_{a2}(0) + \mathbf{R}^T\mathbf{n}_{a2}(\tau) = -\omega_a\mathbf{n}_{a1}(0) \tag{4.21}$$

$$\mathbf{L}^T\mathbf{n}_{b1}(0) + \mathbf{R}^T\mathbf{n}_{b1}(\tau) = \omega_b\mathbf{n}_{b2}(0) \tag{4.22}$$

$$\mathbf{L}^T\mathbf{n}_{b2}(0) + \mathbf{R}^T\mathbf{s}_{b2}(\tau) = -\omega_b\mathbf{n}_{b1}(0) \tag{4.23}$$

The general solution to the differential equation associated with this boundary value problem is

$$\mathbf{n}_{a1}(\sigma) = \cos(\omega_a\sigma)\mathbf{d}_{a1} - \sin(\omega_a\sigma)\mathbf{d}_{a2}$$

$$\mathbf{n}_{a2}(\sigma) = \sin(\omega_a\sigma)\mathbf{d}_{a1} + \cos(\omega_a\sigma)\mathbf{d}_{a2}$$

$$\mathbf{n}_{b1}(\sigma) = \cos(\omega_b\sigma)\mathbf{d}_{b1} - \sin(\omega_b\sigma)\mathbf{d}_{b2}$$

$$\mathbf{n}_{b2}(\sigma) = \sin(\omega_b\sigma)\mathbf{d}_{b2} + \cos(\omega_b\sigma)\mathbf{d}_{b2}$$

Again, these equations are not linearly independent. Four more equations may be generated by orthonormalizing the $\mathbf{n}_{\alpha i}$ and $\mathbf{s}_{\alpha j}$ vectors (conditions on the bilinear form between these vectors):

$$(\mathbf{n}_{a1}, \mathbf{s}_{a1}) = 1, \quad (\mathbf{n}_{a1}, \mathbf{s}_{a2}) = 0 \tag{4.24}$$

$$(\mathbf{n}_{b1}, \mathbf{s}_{b1}) = 1, \quad (\mathbf{n}_{b1}, \mathbf{s}_{b2}) = 0 \tag{4.25}$$

where the bilinear form employed is $(\mathbf{v}, \mathbf{u}) = \mathbf{v}^T(0)\mathbf{u}(0) + \int_{-\tau}^{0} \mathbf{v}^T(\xi + \tau)\mathbf{R}\mathbf{u}(\xi)\mathrm{d}\xi$.

Eqs. (4.11)-(4.14) combined with (4.20)-(4.25) may be solved uniquely for $d_{\alpha ij}$ in terms of the system parameters. Using eqs. (4.19) as the values for $\mathbf{c}_{\alpha i}$ and substituting relevant values of the parameters $\kappa^* = 6.8916$, $\tau^* = 2.9811$, $\omega_a = 1.4427$, and $\omega_b = 2.7726$ [1, 2] yields

$$\mathbf{d}_{a1} = \begin{pmatrix} 0.4786 \\ 0.1471 \end{pmatrix}, \quad \mathbf{d}_{a2} = \begin{pmatrix} -0.4079 \\ 0.1726 \end{pmatrix},$$

$$\mathbf{d}_{b1} = \begin{pmatrix} 0.1287 \\ -0.1088 \end{pmatrix}, \quad \mathbf{d}_{b2} = \begin{pmatrix} 0.1570 \\ 0.0892 \end{pmatrix}$$

4.4 Flow on the Center Manifold

The solution vector $\mathbf{x}_t(\theta)$ may be understood as follows. The center subspace is four-dimensional and spanned by the vectors $\mathbf{s}_{\alpha i}$. The solution vector is decomposed into four components $y_{\alpha i}$ in the $\mathbf{s}_{\alpha i}$ basis, but it also contains a part that is out of the center subspace. This component is infinite-dimensional, and is captured by the term $\mathbf{w} = \begin{pmatrix} w_1 \\ w_2 \end{pmatrix}$ transverse to the center subspace. The solution vector may therefore be written as

$$\mathbf{x}_t(\theta) = y_{a1}(t)\mathbf{s}_{a1}(\theta) + y_{a2}(t)\mathbf{s}_{a2}(\theta) + y_{b1}(t)\mathbf{s}_{b1}(\theta) + y_{b2}(t)\mathbf{s}_{b2}(\theta) + \mathbf{w}(t)(\theta)$$

Note that, by definition,

$$y_{a1}(t) = (\mathbf{n}_{a1}, \mathbf{x}_t)|_{\theta=0} \tag{4.26}$$

$$y_{a2}(t) = (\mathbf{n}_{a2}, \mathbf{x}_t)|_{\theta=0} \tag{4.27}$$

$$y_{b1}(t) = (\mathbf{n}_{b1}, \mathbf{x}_t)|_{\theta=0} \tag{4.28}$$

$$y_{b2}(t) = (\mathbf{n}_{b2}, \mathbf{x}_t)|_{\theta=0} \tag{4.29}$$

The nonlinear part of the operator is crucial for transforming the operator differential equation into the canonical form described by Guckenheimer & Holmes. This nonlinear operator is

$$\mathcal{F}(\mathbf{x}_t)(\theta) = \mathcal{F}(y_{a1}(t)\mathbf{s}_{a1} + y_{a2}(t)\mathbf{s}_{a2} + y_{b1}(t)\mathbf{s}_{b1} + y_{b2}(t)\mathbf{s}_{b2} + \mathbf{w}(t))(\theta)$$

$$= \begin{cases} \mathbf{0} & \theta \in [-\tau, 0) \\ \begin{pmatrix} 0 \\ \frac{\epsilon}{\kappa}(y_{a1}c_{a11} + y_{a2}c_{a21} + y_{b1}c_{b11} \\ +y_{b2}c_{b21} + w_1(t)(0))^3 \end{pmatrix} & \theta = 0 \end{cases}$$

In order to derive the canonical form, we take $\frac{d}{dt}$ of $y_{\alpha i}(t)$ from eqs. (4.26)-(4.29) and carry through the differentiation to the factors of the bilinear form. Noting that $\frac{d}{dt}\mathbf{n}_{\alpha i} = 0$,

$$\begin{aligned}
\dot{y}_{\alpha 1} &= (\mathbf{n}_{\alpha 1}, \dot{\mathbf{x}}_t)|_{\theta=0} = (\mathbf{n}_{\alpha 1}, \mathcal{A}\mathbf{x}_t + \mathcal{F}(\mathbf{x}_t))|_{\theta=0} \\
&= (\mathbf{n}_{\alpha 1}, \mathcal{A}\mathbf{x}_t)|_{\theta=0} + (\mathbf{n}_{\alpha 1}, \mathcal{F}(\mathbf{x}_t))|_{\theta=0} \\
&= (\mathcal{A}^*\mathbf{n}_{\alpha 1}, \mathbf{x}_t)|_{\theta=0} + (\mathbf{n}_{\alpha 1}, \mathcal{F}(\mathbf{x}_t))|_{\theta=0} \\
&= \omega_\alpha(\mathbf{n}_{\alpha 2}, \mathbf{x}_t)|_{\theta=0} + (\mathbf{n}_{\alpha 1}, \mathcal{F}(\mathbf{x}_t))|_{\theta=0} \\
&= \omega_\alpha y_{\alpha 2} + \mathbf{n}_{\alpha 1}^T(0)\mathbf{F}
\end{aligned}$$

and similarly,

$$\dot{y}_{\alpha 2} = -\omega_\alpha y_{\alpha 1} + \mathbf{n}_{\alpha 2}^T(0)\mathbf{F}$$

where $\mathbf{F} = \mathcal{F}(\mathbf{x}_t)(0) = \mathcal{F}(y_{a1}(t)\mathbf{s}_{a1}(0) + y_{a2}(t)\mathbf{s}_{a2}(0) + y_{b1}(t)\mathbf{s}_{b1}(0) + y_{b2}(t)\mathbf{s}_{b2}(0) + \mathbf{w}(t)(0))$, recalling that $\mathcal{F} = \mathcal{F}(\theta)$, and this notation corresponds to setting $\theta = 0$. Substituting in the definition of $\mathbf{n}_{\alpha i}$ and $\mathbf{F}$,

$$\dot{y}_{a1} = \omega_a y_{a2} + \frac{\epsilon d_{a12}(y_{a1} + y_{b1} + w_1)^3}{\kappa} \tag{4.30}$$

$$\dot{y}_{a2} = -\omega_a y_{a1} + \frac{\epsilon d_{a22}(y_{a1} + y_{b1} + w_1)^3}{\kappa} \tag{4.31}$$

$$\dot{y}_{b1} = \omega_b y_{a2} + \frac{\epsilon d_{b12}(y_{a1} + y_{b1} + w_1)^3}{\kappa} \tag{4.32}$$

$$\dot{y}_{b2} = -\omega_b y_{b1} + \frac{\epsilon d_{b22}(y_{a1} + y_{b1} + w_1)^3}{\kappa} \tag{4.33}$$

where we have used eq. (4.19). Recall that the center manifold is tangent to the four-dimensional $y_{\alpha i}$ center subspace at the origin and $\mathbf{w}$ may be approximated by a quadratic in $y_{\alpha i}$. Therefore, the terms w_1 in eqs. (4.30)-(4.33) may be neglected, as their contribution is greater than third order, which had previously

been neglected. To analyze this eqs. (4.30)-(4.33), a van der Pol transformation is applied:

$$
\begin{aligned}
y_{a1}(t) &= r_a(t)\cos(\omega_a t + \theta_a(t)) \\
y_{a2}(t) &= -r_a(t)\sin(\omega_a t + \theta_a(t)) \\
y_{b1}(t) &= r_b(t)\cos(\omega_b t + \theta_b(t)) \\
y_{b2}(t) &= -r_b(t)\sin(\omega_b t + \theta_b(t))
\end{aligned}
$$

which transforms the coupled differential equations (4.30)-(4.33) into

$$
\begin{aligned}
\dot{r}_a = \frac{\epsilon}{\kappa}&(\cos(t\omega_a + \theta_a)r_a + \cos(t\omega_b + \theta_b)r_b)^3 \\
&(d_{a12}\cos(t\omega_a + \theta_a) - d_{a22}\sin(t\omega_a + \theta_a)) \qquad (4.34) \\
\dot{\theta}_a = \frac{-\epsilon}{\kappa r_a}&(\cos(t\omega_a + \theta_a)r_a + \cos(t\omega_b + \theta_b)r_b)^3 \\
&(d_{a22}\cos(t\omega_a + \theta_a) + d_{a12}\sin(t\omega_a + \theta_a)) \qquad (4.35) \\
\dot{r}_b = \frac{\epsilon}{\kappa}&(\cos(t\omega_a + \theta_a)r_a + \cos(t\omega_b + \theta_b)r_b)^3 \\
&(d_{b12}\cos(t\omega_b + \theta_b) - d_{b22}\sin(t\omega_b + \theta_b)) \qquad (4.36) \\
\dot{\theta}_b = \frac{-\epsilon}{\kappa r_b}&(\cos(t\omega_a + \theta_a)r_a + \cos(t\omega_b + \theta_b)r_b)^3 \\
&(d_{b22}\cos(t\omega_b + \theta_b) + d_{b12}\sin(t\omega_b + \theta_b)) \qquad (4.37)
\end{aligned}
$$

By averaging the differential equations (4.34)-(4.37) over a single period of $t\omega_\alpha + \theta_\alpha$, the θ_α dependence of the $\dot{r}_\alpha$ equations may be eliminated. Note that ω_a and ω_b are non-resonant frequencies, so averages may be taken independently of one another.

$$\frac{\omega_a}{2\pi}\int_{\theta_a}^{\theta_a+\frac{2\pi}{\omega_a}} \dot{r}_a \mathrm{d}t = \frac{3}{8}\frac{\epsilon}{\kappa} d_{a12} r_a (2r_b^2 + r_a^2)$$
$$\frac{\omega_b}{2\pi}\int_{\theta_b}^{\theta_b+\frac{2\pi}{\omega_b}} \dot{r}_b \mathrm{d}t = \frac{3}{8}\frac{\epsilon}{\kappa} d_{b12} r_b (2r_a^2 + r_b^2)$$

According to Guckenheimer & Holmes, the normal form for a Hopf-Hopf bifurcation in polar coordinates is

$$\begin{aligned}
\frac{\mathrm{d}r_a(t)}{\mathrm{d}t} &= \mu_a r_a + a_{11} r_a^3 + a_{12} r_a r_b^2 + O(|r|^5) \\
\frac{\mathrm{d}r_b(t)}{\mathrm{d}t} &= \mu_b r_b + a_{22} r_b^3 + a_{21} r_b r_a^2 + O(|r|^5) \\
\frac{\mathrm{d}\theta_a(t)}{\mathrm{d}t} &= \omega_a + O(|r|^2) \\
\frac{\mathrm{d}\theta_b(t)}{\mathrm{d}t} &= \omega_b + O(|r|^2)
\end{aligned}$$

where $\mu_i = \Re\frac{\mathrm{d}\lambda_i(\tau^*)}{\mathrm{d}\tau}$, and τ^* is the critical time-delay for the Hopf-Hopf bifurcation (note that this bifurcation is of codimension-2, so both $\tau = \tau^*$ and $\kappa = \kappa^*$ at the bifurcation). Taking the derivative of the characteristic equation with respect to τ and solving for $\frac{\mathrm{d}\lambda(\tau)}{\mathrm{d}\tau}$ gives

$$\frac{\mathrm{d}\lambda(\tau)}{\mathrm{d}\tau} = \frac{5\lambda(\tau)^2}{5 + 2\exp(\tau\lambda(\tau)) - 5\tau\lambda(\tau) + \exp(\tau\lambda(\tau))\kappa\lambda(\tau)}.$$

Letting $\lambda(\tau) = i\omega_\alpha(\tau)$ and substituting in $\tau = \tau^*$, $\kappa = \kappa^*$, as well as ω_a and ω_b respectively yields

$$\mu_a = -0.1500\Delta \tag{4.38}$$

$$\mu_b = 0.2133\Delta \tag{4.39}$$

where $\Delta = \tau - \tau^*$. This results in the equations for the flow on the center manifold:

$$\dot{r}_a = -0.1500\Delta r_a + 0.0080 r_a(2r_b^2 + r_a^2) \tag{4.40}$$

$$\dot{r}_b = 0.2133\Delta r_b - 0.0059 r_b(2r_a^2 + r_b^2) \tag{4.41}$$

To normalize the coefficients and finally obtain the flow on the center manifold in normal form, let $\bar{r}_a = r_a\sqrt{0.0080}$ and $\bar{r}_b = r_b\sqrt{0.0059}$, resulting in:

$$\dot{\bar{r}}_a = -0.1500\Delta\bar{r}_a + \bar{r}_a^3 + 2.7042\bar{r}_a\bar{r}_b^2$$

$$\dot{\bar{r}}_b = 0.2133\Delta\bar{r}_b - 1.4792\bar{r}_a^2\bar{r}_b - \bar{r}_b^3$$

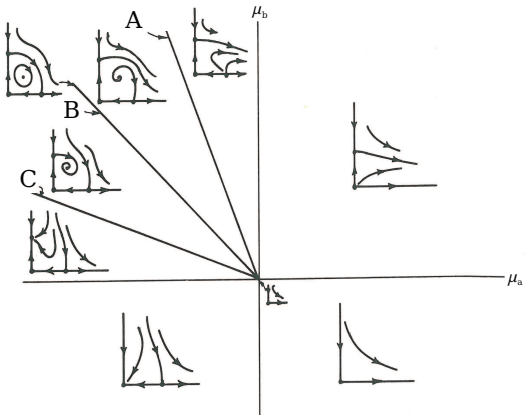

Figure 4.1: Partial bifurcation set and phase portraits for the unfolding of this Hopf-Hopf bifurcation. After Guckenheimer & Holmes [17] Figure 7.5.5. Note that the labels A : $\mu_b = a_{21}\mu_a$, B : $\mu_b = \mu_a(a_{21} - 1)/(a_{12} + 1)$, C : $\mu_b = -\mu_a/a_{12}$.

This has quantities $a_{11} = 1$, $a_{22} = -1$, $a_{12} = 2.7042$, and $a_{21} = -1.4792$, which implies that this Hopf-Hopf bifurcation has the unfolding illustrated in Figure 4.1.

For the calculated a_{ij}, the bifurcation curves in Figure 4.1 become A : $\mu_b = -1.4792\mu_a$, B : $\mu_b = -.6992\mu_a$, and C : $\mu_b = -.3697\mu_a$. From eqs. (4.38)-(4.39), system (4.1) has $\mu_b = -1.422\mu_a$ for the given parameter values. Comparison with Figure 4.1 shows that this implies the system exhibits two limit cycles with saddle-like stability and an unstable quasiperiodic motion when $\Delta > 0$. We note that the center manifold analysis is local and is expected to be valid only in the neighborhood of the origin.

For comparison, the center manifold reduction eqs. (4.40), (4.41) predict three solutions bifurcating from the Hopf-Hopf (the trivial solution notwithstanding):

$$(r_a, r_b) = \begin{cases} \left(4.3295\sqrt{\Delta}, 0\right) & (4.42) \\ \left(0, 6.0020\sqrt{\Delta}\right) & (4.43) \\ \left(4.2148\sqrt{\Delta}, 0.6999\sqrt{\Delta}\right) \quad \text{(quasiperiodic)} & (4.44) \end{cases}$$

We note that eqs. (4.42), (4.43) are the same as obtained via Lindstedt's Method in the previous section.

4.5 Continuation

Figure 4.2 shows a plot of these results along with those obtained from numerical continuation of the original system (4.1) with the software package DDE-BIFTOOL[13]. Note that only the two limit cycles are plotted for comparison. The numerical method is seen to agree with the periodic motions predicted by Lindstedt's Method and center manifold reduction.

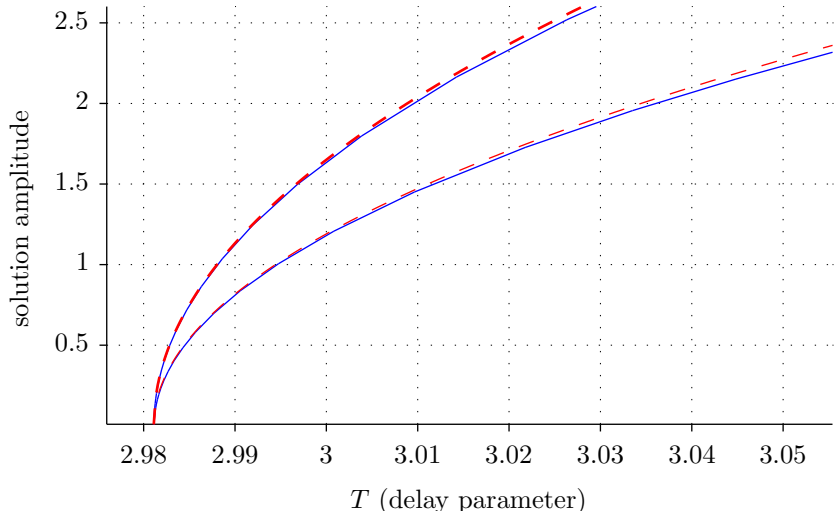

Figure 4.2: Comparison of predictions for the amplitudes of limit cycles bifurcating from the Hopf-Hopf point in eq. (4.1) obtained by (a) numerical continuation of eq. (4.1) using the software DDE-BIFTOOL (solid lines) and (b) center manifold reduction, eqs. (4.42), (4.43) (dashed lines).

4.6 Conclusion

This work has demonstrated agreement between Lindstedt's Method for describing the amplitude growth of limit cycles after a Hopf-Hopf bifurcation and the center manifold reduction of a Hopf-Hopf bifurcation in a nonlinear differential delay equation. While the center manifold reduction analysis is considerably more involved than the application of Lindstedt's Method, it does uncover the quasiperiodic motion which neither Lindstedt's Method nor numerical continuation revealed. Note that in addition to the two limit cycles which were expected to occur due to the Hopf-Hopf bifurcation, the codimension-2 nature of this bifurcation has introduced the possibility of more complicated dynamics than originally anticipated, namely the presence of quasiperiodic motions. This work has served to rigorously show that a system inspired by the physi-

cal application of delay-coupled microbubble oscillators exhibits quasiperiodic motions because in part of the occurrence of a Hopf-Hopf bifurcation.

CHAPTER 5

CONCLUSION

In this research, we have analyzed the behavior of the Rayleigh-Plesset Equation with delay coupling. The research has been conducted through the lens of coupled nonlinear oscillators, and as such the questions addressed have included "do the oscillators synchronize?" and "is vibration a stable motion?" Perturbation methods and numerical methods were employed to shed light on these questions, and model simplifications have been used to explore complicated phenomena at longer delay.

The focus of this research has been the dynamics, stability and bifurcations of the in-phase mode; in particular, when does the in-phase mode exist, and for what values of delay is it stable? It has been shown that not only is the in-phase mode stable when initial conditions are chosen on the in-phase manifold, but also when chosen away from the in-phase manifold. Therefore, the oscillatory behavior that can exist for certain "windows" of delay is stable even for general initial conditions.

Of particular interest is the existence of a Hopf-Hopf bifurcation of the in-phase mode for particular initial conditions. This was found to be possible because of the two infinite sequences of Hopf bifurcations that switch relative position for increasing delay. This codimension-2 bifurcation was studied via center manifold reductions on an analogous system. Whereas numerical integration of the coupled Rayleigh-Plesset equations showed quasiperiodic solutions, so were such motions predicted by the unfolding of the Hopf-Hopf bifurcation. Therefore, for reasonably long time delays, the behavior of the two coupled bubble oscillators has been mapped out.

Future work in delay-coupled bubble oscillators would include the introduction of higher-order correction terms to the coupling function, as well as modeling the translational dynamics of bubble oscillators. It is known that in a fluid, the translational motion of bubbles is strongly influenced by the radius of the bubble via such forces as, e.g. viscosity (proportional to the cross-sectional area of the bubble) and inertial fluid effects proportional to the volume of the bubble (also known as "added mass"). However, just as delay effects have been largely neglected to date in modeling the radius of bubbles, so have they been ignored in their effects on translational modeling. It is conceivable that since such bifurcations in radial motion are predicted by this research, so should delay give rise to rich behavior in the translational dynamics of coupled microbubbles.

APPENDIX A

LINDSTEDT'S METHOD SECOND-ORDER CORRECTIONS

The coefficients B,C and D in eq.(2.28) are found to be as follows:

$$
\begin{aligned}
B &= [\sin(\omega_{cr}T_{cr})(8A^2cP\omega_{cr}^4 - 2A^2cP^2\omega_{cr}^2 - 24A^2cP\omega_{cr}^2) \\
&+ \cos(2\omega_{cr}T_{cr})(-3A^2c^2P\omega_{cr}^3 - 8A^2P\omega_{cr}^3 - 28A^2c^2P\omega_{cr}) \\
&+ \cos(\omega_{cr}T_{cr})(-8A^2c^2P\omega_{cr}^3 - 16A^2P\omega_{cr}^3 + 8A^2c^2P\omega_{cr}) \\
&+ 24A^2cP\sin(2\omega_{cr}T_{cr})\omega_{cr}^2 - 2A^2cP^2\omega_{cr}^3 - 120A^2c^2\omega_{cr}^3 - 64A^2\omega_{cr}^3 - 128A^2c^2\omega_{cr}] \\
&\quad /[64c^3\omega_{cr}^2(\omega_{cr}^2 - 2) + 4cP^2\omega_{cr}^2 + 64c\cos(2\omega_{cr}T_{cr})P\omega_{cr}^2 \\
&+ 32c^2P\sin(2\omega_{cr}T_{cr})\omega_{cr}(1 - \omega_{cr}^2) + 64c(c^2 + 4\omega_{cr}^2)] \qquad \text{(A.1)} \\
C &= [\cos(\omega_{cr}T_{cr})(8A^2cP\omega_{cr}^4 - 24A^2cP\omega_{cr}^2) \\
&+ \sin(\omega_{cr}T_{cr})(-2A^2P^2\omega_{cr}^3 + 8A^2c^2P\omega_{cr}^3 + 16A^2P\omega_{cr}^3 - 8A^2c^2P\omega_{cr}) \\
&+ \sin(2\omega_{cr}T_{cr})(-3A^2c^2P\omega_{cr}^3 - 8A^2P\omega_{cr}^3 - 28A^2c^2P\omega_{cr}) - 24A^2c\cos(2\omega_{cr}T_{cr})P\omega_{cr}^2 \\
&+ 100A^2c^3\omega_{cr}^2 - 224A^2c\omega_{cr}^2 - 112A^2c^3 + 12A^2c^3\omega_{cr}^4 + 32A^2c\omega_{cr}^4 - 2A^2cP^2\omega_{cr}^2] \\
&\quad /[64c^3\omega_{cr}^2(\omega_{cr}^2 - 2) + 4cP^2\omega_{cr}^2 + 64c\cos(2\omega_{cr}T_{cr})P\omega_{cr}^2 \\
&+ 32c^2P\sin(2\omega_{cr}T_{cr})\omega_{cr}(1 - \omega_{cr}^2) + 64c(c^2 + \omega_{cr}^2)] \qquad \text{(A.2)} \\
D &= \frac{-A^2}{16c^2}(2\cos(\omega_{cr}T)P\omega_{cr}^2 - 2cP\sin(\omega_{cr}T)\omega_{cr} - 28c^2 + 3c^2\omega_{cr}^2 + 8\omega_{cr}^2) \qquad \text{(A.3)}
\end{aligned}
$$

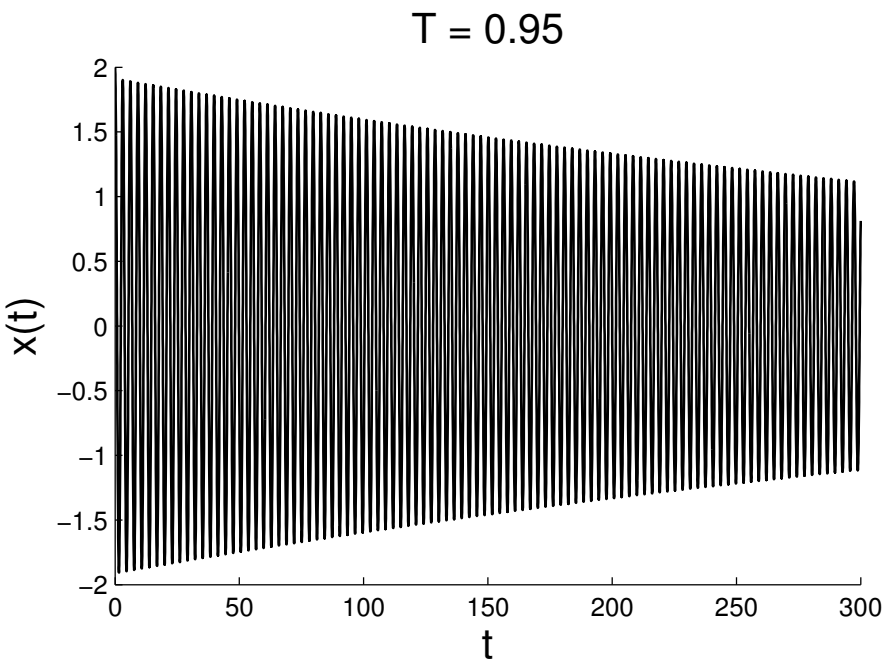

Figure A.1: Numerical integration of the linearized eq.(2.4) for the parameters of eq.(2.5) with delay $T = 0.95$. Note that the equilibrium is stable.

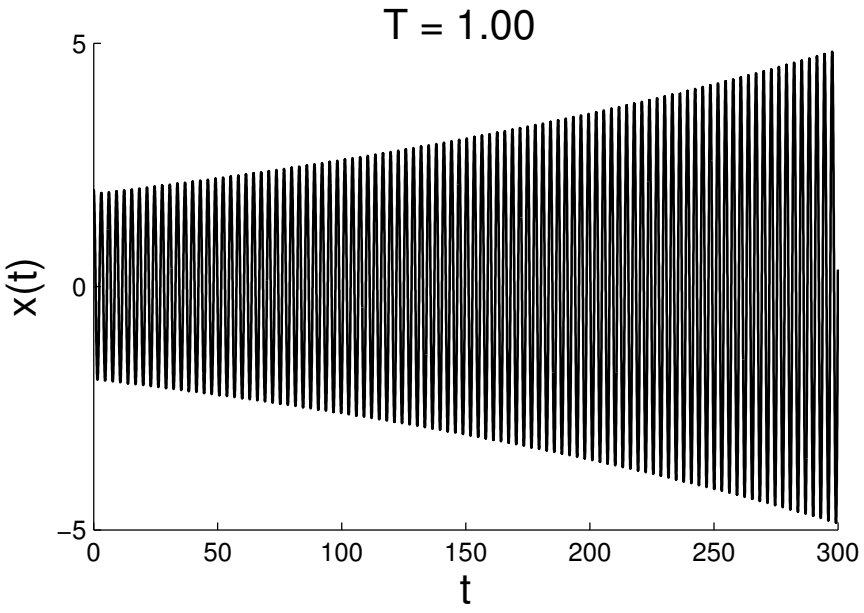

Figure A.2: Numerical integration of the linearized eq.(2.4) for the parameters of eq.(2.5) with delay T=1.00. Note that the equilibrium is unstable.

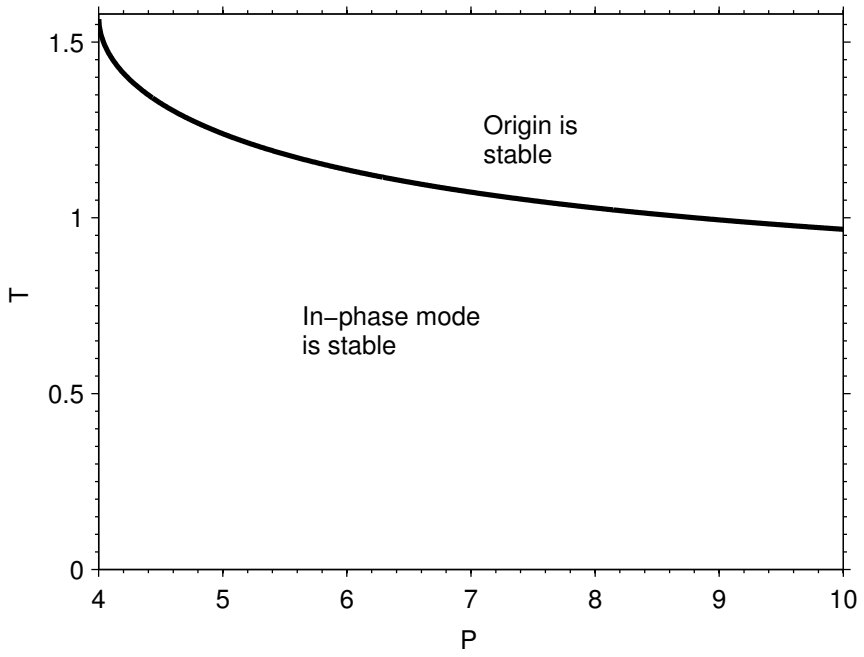

Figure A.3: T_{cr} versus P for parameters $c = 94$ and $\gamma = \frac{4}{3}$, from eq. (2.13). For $T > T_{cr}$ and $P > 3\gamma$ the origin is unstable and a bounded periodic motion (a limit cycle) exists, having been born in a Hopf bifurcation.

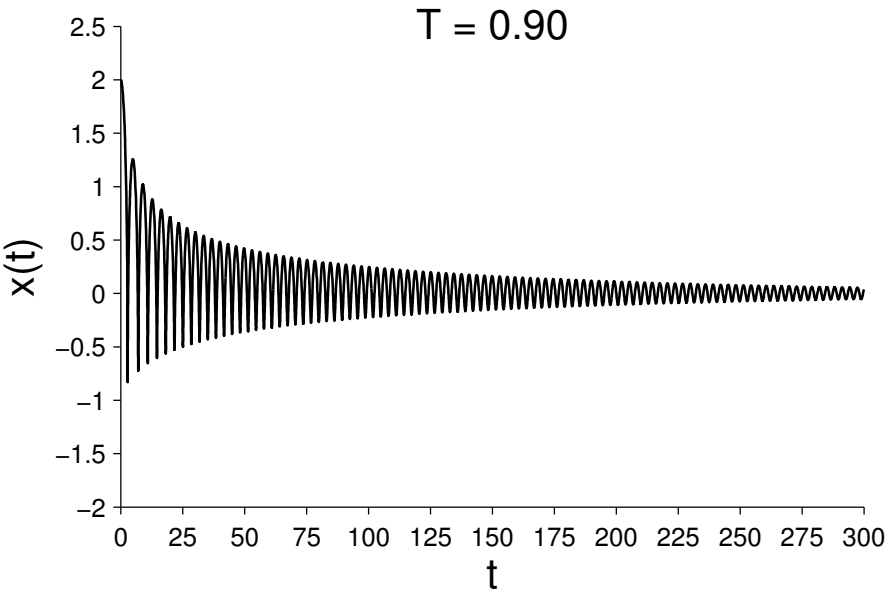

Figure A.4: Numerical integration of eq.(2.3) for the parameters of eq.(2.5) with delay $T = 0.90$. Note that the equilibrium is stable.

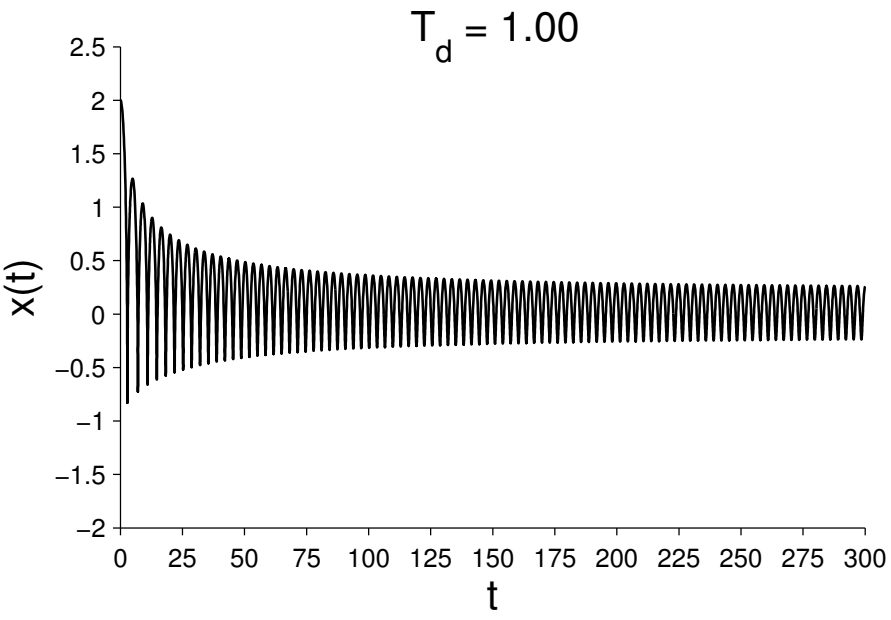

Figure A.5: Numerical integration of eq.(2.3) for the parameters of eq.(2.5) with delay $T = 1.00$. Note that the equilibrium has become unstable, but that a bounded periodic motion exists indicating a Hopf bifurcation.

APPENDIX B

NUMERICAL CONTINUATION USING DDE-BIFTOOL

In the several figures, results from the delay-differential equation continuation software `DDE-BIFTOOL` are displayed. This appendix serves as a simple walk-through on how the software may be used to recreate the results in the above figure. Please note that the software package comes with an official series of tutorials and examples that are helpful in demonstrating even more functionality that has not been used in my analysis.

B.1 Numerical Continuation

The primary purpose of numerical continuation is to follow the behavior of a specific solution or bifurcation as parameters are varied in the system. Numerical continuation by definition makes use of software, the implicit function theorem, and the existence and uniqueness theorem for solutions to differential equations. A basic example of numerical continuation is in the context of ordinary differential equations. In this scenario, one is given a system

$$\dot{\boldsymbol{x}} = \boldsymbol{f}(\boldsymbol{x}, \lambda), \quad \boldsymbol{x} \in \mathbb{R}^n, \quad \lambda \in \mathbb{R} \tag{B.1}$$

where $f(\mathbf{x}, \lambda)$ is a smooth function and λ is a parameter, that has an equilibrium solution

$$\boldsymbol{f}(\boldsymbol{x_0}, \lambda_0) = 0, \tag{B.2}$$

noting that this solution may vary in value with λ. Following the numerical value of this equilibrium solution is the basic goal of a numerical continuation routine. While doing this, bifurcations of the equilibrium point may be detected by also analyzing the spectrum of the equilibrium; stability information may also be calculated in this process.

The continuation process carried out on an equilibrium point is guaranteed to result in a branch of equilibrium points as long as the Jacobian matrix for the equilibrium point is nondegenerate, i.e. that it has maximal rank. For a one-dimensional differential equation, that means that there exists a branch $\boldsymbol{x}(\lambda)$ for which $\boldsymbol{x}(\lambda_0) = \boldsymbol{x_0}$ and $f(\boldsymbol{x}(\lambda), \lambda) = 0$. To "build up" the branch, a new parameter value close to the previous $\lambda_1 = \lambda_0 + \epsilon$ and the differential equation is evaluated at $\boldsymbol{x_0}$. A root-finding algorithm such as Newton's Method is applied in order to calculate the new position of the equilibrium point. Codimension-1 bifurcations may be detected along the branch by analyzing the Jacobian for singularities. In order to follow an equilibrium point around folds where the derivative is infinite, distance *along the branch* is used as the independent variable for a solution—the details of such a formulation are available from, e.g. Kuznetsov [24] §10.2.

The process may be extended to continuation of periodic orbits. Here, the computation is similar to the case of an equilibrium point, except that fixed points of the Poincaré Map are continued. The Floquet multipliers and period of the periodic orbit are also calculated in this process, so bifurcations in the limit cycle may be detected by inspection of those quantities.

In this work, numerical continuation is used as a tool to confirm perturbation results and explore exciting phenomena. Numerical continuation in delay-

differential equations is explored in detail by Engelborghs [14], who also wrote a package for MATLAB to perform these computations named DDE-BIFTOOL. The process of applying this package to the Rayleigh-Plesset Equation is described in detail in the following sections.

B.2 Installation

The installation files for DDE-BIFTOOL can be retrieved from http://twr.cs.kuleuven.be/research/software/delay/ddebiftool.shtml. The function and runtime files used in this walkthrough are available at http://www.math.cornell.edu/~rand/randdocs/Heckman_DDEBiftool.

Follow the link to the "warranty and download" page, and download the version 2.03 ZIP archive. Upon unzipping the file, a new directory "DDE-BIFTOOL_203" is created. In it, there are three more sets of archives, a readme, and an addendum manual. The set of ZIP archives named TW330.p*.zip contains the full manual for the tool, replete with descriptions of each major function included, data structures used, and a walk-through for the packaged demos in PostScript and PDF format. Reading through this manual is strongly recommended for the beginner in continuation, DDEs, or those relatively unfamiliar with the MATLAB programming language.

The next archive is named ddbiftool.zip. Unpackaging it will create a new directory named ddebiftool, which contains all of the resources that comprise the tool. This folder should be placed somewhere that is already in the MATLAB path, or should be added to the path manually. The way to accomplish this via the MATLAB GUI is dependent on the user's version of MATLAB,

but it may be also accomplished by using the `path` command (for more on the command, read the on-line help: `help path`).

Finally, the archive named `system.zip` contains a directory named `system`, under which there are three more directories full of demonstration systems. "System files" and runtime files (those extracted from `ddebiftool.zip`) should be kept in separate directories, and in particular the working directory should be set to the folder of the system on which the user is operating. Therefore, to run the main demo for `DDE-BIFTOOL`, the working directory should be changed to the `demo` folder under `system`. New systems may be created in arbitrary locations in the user's filesystem as a result.

B.3 System Functions

There are a number of resource files that must first be created in a separate directory before commands may be run in MATLAB to start the computation. Place the following files in their own folder, separate from the `DDE-BIFTOOL` runtime files. By default, the software unpacks a folder named `system` in which a number of tutorials are located; a new folder under this directory is an appropriate location for these new system files.

The first file that must be written is the system definition file, `sys_rhs.m`.

```
function f=sys_rhs(xx,par)

x = xx(1,1);                % state variable
xd = xx(2,1);               % first derivative of state variable
xl = xx(1,2);               % state variable, time lagged
xld = xx(2,2);              % derivative of time-lag state var.
```

```
e = 1;                          % arbitrary value of epsilon
k = 6.8915;                     % slightly-detuned from Hopf-Hopf

f(1,1) = xd;                    % the system of ODEs
f(2,1) = -(4/k)*xd - 4*x - (10/k)*xld + (e/k)*x.^3;

return;
```

sys_rhs.m

Another file needed is `sys_tau.m`. This file designates "which parameter" is the delay parameter in the system. Note that `DDE-BIFTOOL` can support multiple delay parameters. However, the software *does not have a central listing* of these parameters for each system; they are provided in an anonymous fashion within `sys_rhs` and are designated by handles e.g. `par(i)`, where `i` is consistent across all references to a particular parameter. In this system, there is only *one* parameter, and that parameter *is* the delay parameter. Therefore, the file `sys_tau.m` could not be any simpler:

```
function tau=sys_tau()

% T

tau=[1];

return;
```

sys_tau.m

The next file that must be established calculates the Jacobian (partial derivatives with respect to state variables and parameters). This has the file-

name `sys_deri.m`. In many cases, it suffices to use a default file provided with `DDE-BIFTOOL` that calculates these partial derivatives numerically (`df_deriv.m`, found in the package's root directory). I will make use of that method in my computations, rather than writing a custom Jacobian resource file.

For the continuation to work, the files `sys_ntau.m` and `sys_init.m` must also be copied. The latter file should be modified to have a correct directory traversal with respect to the current directory, as well as an appropriate "name" for the system. For this system, these files are:

```
1 function []=sys_ntau()

3 error('SYS_NTAU: This sys_ntau is a dummy file!');

5 return;
```

sys_ntau.m

```
function [name,dim]=sys_init()
2
name='dummy';
4 dim=2;
path(path,'../../ddebiftool/');
6
return;
```

sys_init.m

B.4 Runtime scripts

The simplest way to run the software package is by scripting the commands in an m-file. Below is a list of the commands used to generate the figure in this paper, with comments interspersed to explain what the commands are doing.

This clears the workspace and initializes the system handle:

```
clear all
[name,n]=sys_init;
```

Next, this identifies the bifurcation parameter continuation domain, and the initial step size to use for the bifurcation parameter. Note that since this system only uses the time delay as the bifurcation parameter, the variables begin with "delay;" this is not required.

```
delay_begin = 2;
delay_end = 4;
delay_step = 0.0001;
```

Beyond the creation of double-precision integer arrays, MATLAB also facilitates the organized storage of data by use of the `struct` class. Note that in the call to `stst.kind='stst'`, the *first* instance of `stst` is the *name* of the variable, and the *second* is the *kind* of object. From a MATLAB data structure perspective, the structure `stst` is being created, with one of its fields (`kind`) being set to the string `stst` as well.

```
stst.kind='stst';
```

```
stst.parameter=delay_begin; % first parameter value
stst.x=[0 0]';  % approx ic's for eq. pt.
method=df_mthod('stst');
[stst,success]=p_correc(stst,[],[],method.point);
```

Next, the field `paramter` is set for the variable `stst`, and it is specified as the parameter value previously assigned to `delay_begin`. Finally, the command `stst.x=[0 0]'` assigns an *approximate* location of an equilibrium point to the variable `stst`. It turns out in this case that this is the exact location of the equilibrium point, but this is only verified after `p_correc`, a function that is part of the tool. The command preceding sets the correction method to look for an equilibrium point.

```
method.stability.minimal_real_part=-50;
```

There are an infinite number of complex roots to a differential delay equation's characteristic equation. However, an infinite number will have negative real part, and only a finite number will have positive real part. Therefore, since we are mostly concerned about the roots as they cross the imaginary axis for stability purposes, we may sensibly ignore those roots that are very far away from it. This setting specifies the minimum real part needed (i.e. the largest negative real part) for `DDE-BIFTOOL` to calculate the root.

This command will calculate the stability of the equilibrium point `stst` and set `stability` as a new field of `stst` to the calculation output.

```
stst.stability=p_stabil(stst,method.stability);
```

The next command plots a locus of roots for the equilibrium point `ststst` in the complex plane. Note that first a predictive step for the roots is taken, followed by a corrective step. Red roots designate positive real part which lead to asymptotic instability. This is demonstrated in Figure B.1.

```
figure(1); clf; p_splot(ststst)
```

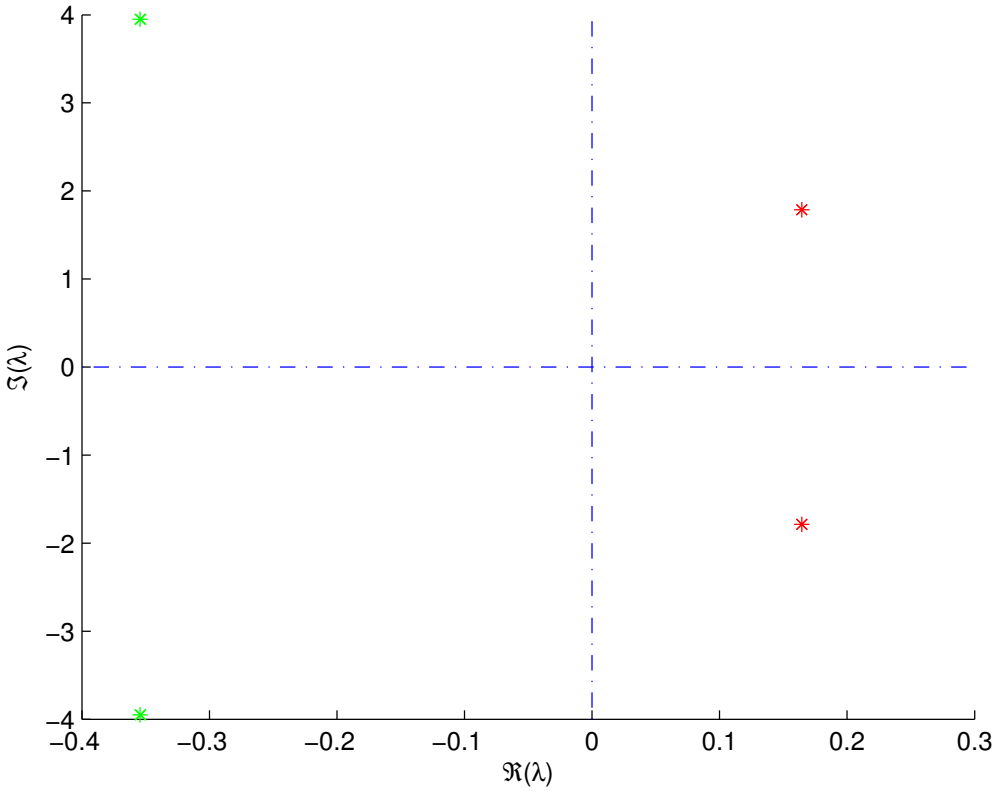

Figure B.1: Plot of eigenvalues of the origin in the complex plane as produced by p_splot during runtime.

Central to continuation is the concept of a "branch." This is a collection of solutions wherein the continuation parameter is varied slightly and the perturbed solution is calculated. This creates a sequence of objects (equilibrium points, limit cycles, etc.) that are topologically equivalent. Should branches have a definite "beginning" or "ending," they are located at bifurcation points.

The below sequence of commands is used to build up the branch of equilibrium points starting at `stst` via continuation. First, a branch object is created and named `branch1`. It is designated to have as the continuation parameter the "first parameter" in the list (in this system, there is only one parameter—the delay), and that it will be a branch of equilibrium points. The `max_bound` and `max_step` fields set the maximum bound and initial step size for the continuation parameter, respectively. Note the first entry in the input vectors are `1`, the "parameter position;" for continuation of the same system in more than one variable, other branches will have a different value depending on the parameter of interest.

```
branch1 = df_brnch(1,'stst'); % first (and only) parameter (delay)
branch1.parameter.max_bound = [1 delay_end]; % 1 is the parameter
    pos.
branch1.parameter.max_step  = [1 delay_step]; % same as above
branch1.point(1) = stst; % start with the steady state point
    determined
stst.parameter = delay_begin+delay_step;
[stst,success]=p_correc(stst,[],[],method.point);
branch1.point(2)=stst; % next branch point is as calculated
```

Next, the branch is given a starting point—in this case, the original trivial

equilibrium point designated earlier in `stst`. The data from the variable `stst` is copied into `branch1.point(1)`. With that information integrated into the branch, the next command increases the delay parameter slightly and the equilibrium, followed by recalculating the point position in case it has changed due to the new parameter value (in this case it will not move, since this is a trivial equilibrium point). This new equilibrium point is also copied into the branch as `branch1.point(2)`.

```
branch1.method.continuation.plot=0;
[branch1,s,f,r]=br_contn(branch1,50000);
```

The first command above turns off plotting when running continuation on this branch; this is sensible here because the branch is trivial, and the plot output would identify a solution with zero amplitude for the range of continuation.

The second command runs the continuation routine on the branch, for as many as 50,000 iterations or until the maximum parameter bound defined in `branch1.parameter.max_bound` is reached. This will populate the structure `branch1` with equilibrium points whose location is recalculated at each new parameter value, sufficing for trivial and nontrivial equilibrium points.

Many of the functions that act on `point` data types also have analogous counterparts for `branch` data types; for instance, whereas `p_stabil` calculates the stability of a single point, `br_stabl` calculates the stability of each point that is within a branch. This will assign new stability information to the branch point-by-point, and is used to identify bifurcation points. Note that the prepackaged version of the function contains a safety check that has been disabled for this calculation.

```
branch1 = br_stabl(branch1,0,1);
```

Equipped with the stability of the equilibrium point along the branch, we know that changes in stability will correspond to bifurcations. The function to locate Hopf points is `p_tohopf`; it takes an "initial guess" of an equilibrium point that is undergoing Hopf bifurcation as input, and as output returns a machine-precision approximation for the location of a Hopf point. Here, it is output first as the variable `hopf`, and then renamed to `first_hopf` to distinguish itself from later Hopf bifurcations. Note that if there are multiple Hopf points close to one another, the initial approximation point will have to be precisely chosen.

```
hopf=p_tohopf(branch1.point(10));
method=df_mthod('hopf');
[hopf,success]=p_correc(hopf,1,[],method.point);
first_hopf=hopf;
```

With a Hopf point identified, a natural next step would be to characterize the periodic solution that bifurcates from the equilibrium point. In particular, what is the amplitude-parameter dependence of the limit cycle? Whereas this is a computationally expensive and tedious exercise using numerical integration, continuation is uniquely equipped to quickly calculate limit cycle profiles via calculating fixed points of Poincaré maps.

Two separate points along the periodic solution are required to build up a branch of periodic solutions. In the below code, those two points are `psol` and

`deg_psol`. The latter corresponds to the periodic solution *exactly corresponding* to the Hopf point `first_hopf`, and the former to a slightly detuned point from the Hopf. Lines 1–3 above establish a point along the periodic solution branch `psol` by making a guess at the periodic solution using a polynomial of degree 3. The function `p_corrc` is then employed to correct the location of the periodic solution. Separately, a new (empty) branch for the periodic solution `branch2` is initialized and parameter bounds are set. Finally, `deg_psol` is calculated, coincident with the Hopf point. The data from `deg_psol` and `psol` are copied to `branch2`, and the function `br_contn` runs the continuation calculation.

The result is a branch full of points corresponding to the periodic solution that had bifurcated from `first_hopf`; this is shown in Figure B.2.

```
intervals=20;
degree=3;
[psol,stepcond]=p_topsol(first_hopf,1e-4,degree,intervals);
method=df_mthod('psol');
[psol,success]=p_correc(psol,1,stepcond,method.point); % correction
branch2=df_brnch(1,'psol');
branch2.parameter.max_bound=[1 delay_end];
branch2.parameter.max_step=[1 .01]; % custom
deg_psol=p_topsol(first_hopf,0,degree,intervals);
deg_psol.mesh=[]; % save memory by clearing the mesh field
branch2.point=deg_psol;
psol.mesh=[];
branch2.point(2)=psol;
figure(23);
[branch2,s,f,r]=br_contn(branch2,100);
```

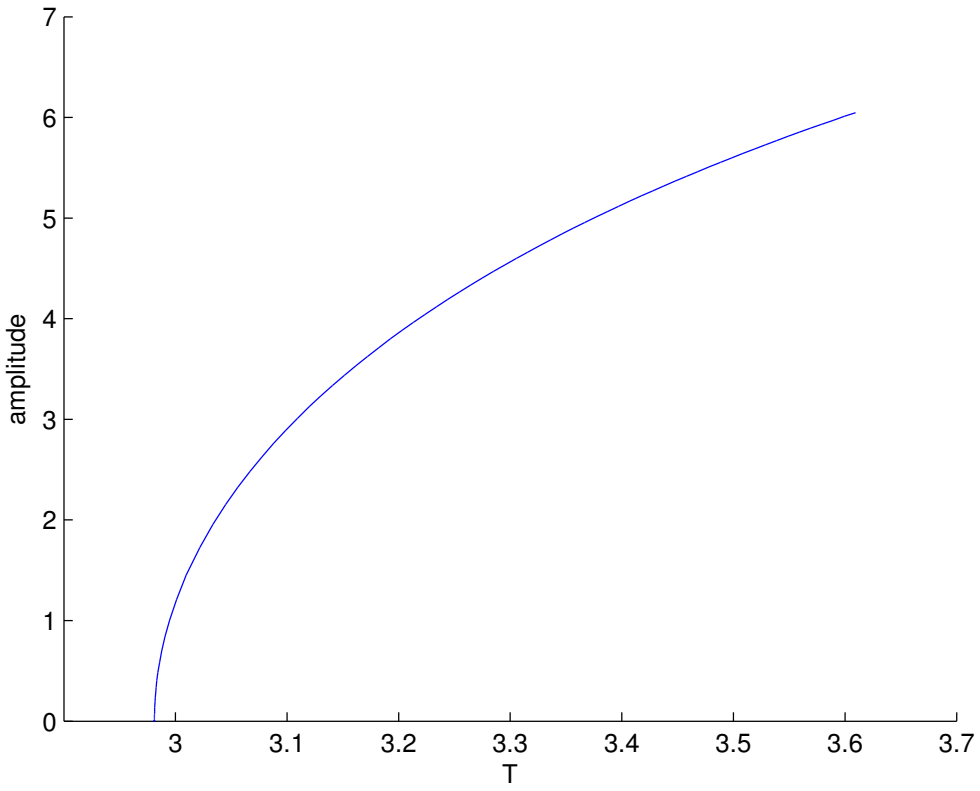

Figure B.2: Continuation output of the first nontrivial branch as generated by br_contn.

This particular system is almost degenerate—the first and second Hopf bifurcations are tuned to occur at parameter values that are very close to one another. It turns out too that the numerical algorithm that locates the Hopf bifurcations (`p_tohopf`) often settles on one Hopf bifurcation far more often than the other. As a result, finding *both* Hopf points can be difficult. The script `find_hopf.m` is a suggestion of how to find a Hopf point unique from the first one by comparing the frequencies, and is provided below.

```
pt = 1;
w0 = first_hopf.omega;
second_hopf.omega = w0;
```

```
while abs(second_hopf.omega - w0) < 0.1 && pt < length(branch1.point)
    pt = pt + 1;
    hopf = p_tohopf(branch1.point(pt));
    method=df_mthod('hopf');
    [hopf,success]=p_correc(hopf,1,[],method.point);
    second_hopf = hopf;
    hopf.stability=p_stabil(hopf,method.stability);
end
```

find_hopf.m

With the second Hopf point found at index `pt`, the branch is then built up as before; first, the new Hopf point is identified and corrected.

```
hopf = p_tohopf(branch1.point(pt));
method=df_mthod('hopf');
[hopf,success]=p_correc(hopf,1,[],method.point);
second_hopf = hopf;
hopf.stability=p_stabil(hopf,method.stability);
```

The rest of the continuation follows exact as that done on `branch2` above, except all bifurcating from `second_hopf` rather than `first_hopf`. Below is the script that accomplishes this, and the output is displayed in Figure B.3.

```
intervals=20;
degree=3;
[psol,stepcond]=p_topsol(second_hopf,1e-4,degree,intervals);
method=df_mthod('psol');
[psol,success]=p_correc(psol,1,stepcond,method.point); % correction
branch3=df_brnch(1,'psol');
```

```
branch3.parameter.max_bound=[1 delay_end];
branch3.parameter.max_step=[1 .01];
deg_psol=p_topsol(second_hopf,0,degree,intervals);
deg_psol.mesh=[]; % save memory by clearing the mesh field
branch3.point=deg_psol;
psol.mesh=[];
branch3.point(2)=psol;
figure(23);
[branch3,s,f,r]=br_contn(branch3,100);
```

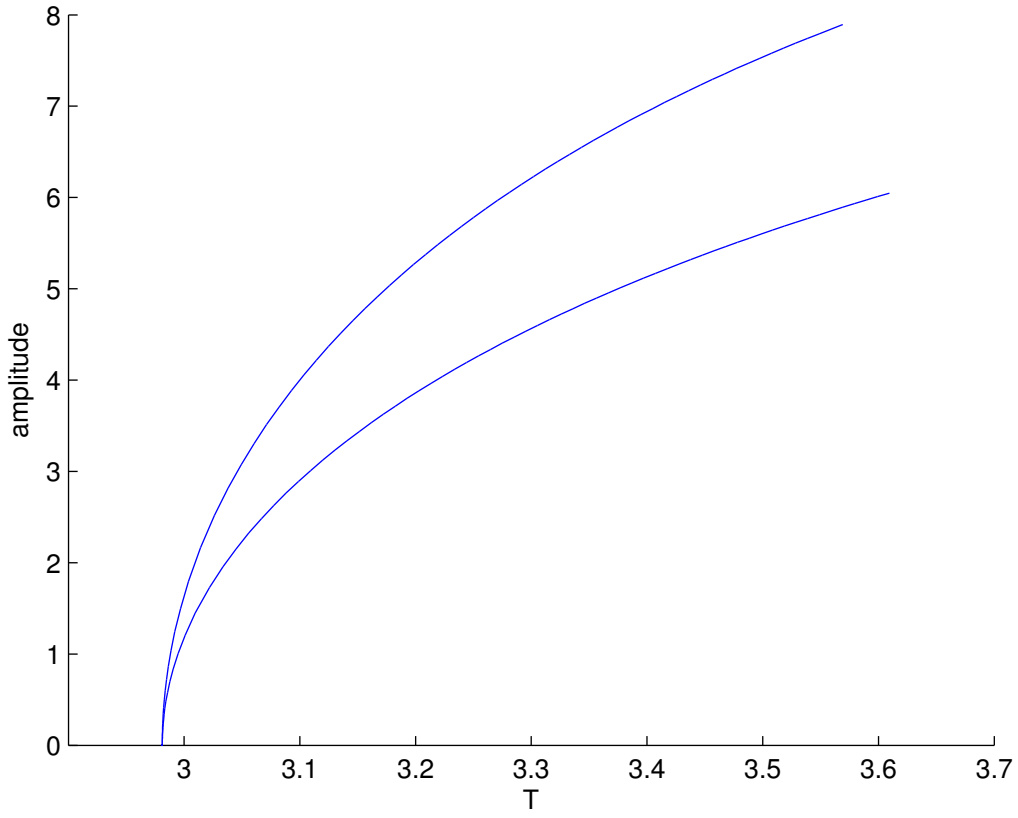

Figure B.3: Continuation output of the second nontrivial branch as generated by br_contn. Note that this branch bifurcates from the same Hopf point but generates a different amplitude prediction, due to the Hopf point's degeneracy.

BIBLIOGRAPHY

[1] C. R. Heckman, J. Kotas, and R. H. Rand. Center manifold reduction of the hopf-hopf bifurcation in a time delay system. *The First International Conference on Structural Nonlinear Dynamics and Diagnosis*, 2012.

[2] C. R. Heckman, J. Kotas, and R. H. Rand. Center manifold reduction of the hopf-hopf bifurcation in a time delay system. *European Society of Applied and Industrial Mathematics Proceedings*, to appear.

[3] C. R. Heckman and R. H. Rand. Dynamics of coupled microbubbles with large fluid compressibility delays. *European Nonlinear Oscillations Conference*, 2011.

[4] C. R. Heckman and R. H. Rand. Dynamics of microbubble oscillators with delay coupling. *Nonlinear Dynamics*, in review.

[5] C. R. Heckman and Rand R.H. Asymptotic analysis of the hopf-hopf bifurcation in a time-delay system. *Journal of Applied Nonlinear Dynamics*, 1:159–171, 2012.

[6] C. R. Heckman, S. M. Sah, and R. H. Rand. Dynamics of microbubble oscillators with delay coupling. *Communications in Nonlinear Science and Numerical Simulation*, 15:2735–2743, 2010.

[7] R. H. Rand and C. R. Heckman. Dynamics of coupled bubble oscillators with delay. *American Society of Mechanical Engineers IDETC/CIE*, 2009.

[8] P. L. Buono and J. Bèlair. Restrictions and unfolding of double hopf bifurcation in functional differential equations. *Journal of Differential Equations*, 189:234–266, 2003.

[9] Z. Chen and P. Yu. Double-hopf bifurcation in an oscillator with external forcing and time-delayed feedback control. *ASME International Design and Engineering Technical Conferences*, 2005.

[10] P. A. Dijkmans. Microbubbles and ultrasound: from diagnosis to therapy. *European Journal of Echocardiology*, 5:245–256, 2004.

[11] A. A. Doinikov, R. Manasseh, and A. A. Ooi. Time delays in coupled multibubble systems. *Journal of the Acoustical Society of America*, 117:47–50, 2005.

[12] Eusebius Doedel *et al.* AUTO: Software for continuation and bifurcation problems in ordinary differential equations. `http://indy.cs.concordia.ca/auto/`, 2007.

[13] K. Engelborghs, T. Luzyanina, G. Samaey, D. Roose, and K. Verheyden. Dde-biftool. `http://twr.cs.kuleuven.be/research/software/delay/ddebiftool.shtml`, 2010.

[14] K. Engelborghs and D. Roose. Numerical computation of stability and detection of hopf bifurcations of steady state solutions of delay differential equations. *Advances in Computational Mathematics*, 10:271–289, 2000.

[15] K. Ferrara, R. Pollard, and M. Borden. Ultrasound microbubble contrast agents: fundamentals and application to gene and drug delivery. *Annual Review of Biomedical Engineering*, 9:415–447, 2007.

[16] F.R. Gilmore. The growth or collapse of a spherical bubble in a viscous compressible liquid. Technical Report 26-4, Hydrodynamics Laboratory, California Institute of Technology, Pasadena, California, 1952.

[17] J. Guckenheimer and P. Holmes. *Nonlinear Oscillations, Dynamical Systems, and Bifurcations of Vector Fields*. Springer, 1983.

[18] J. Guckenheimer and Y. A. Kuznetsov. Hopf-hopf bifurcation. *Scholarpedia*, 3:1856, 2008.

[19] A. Harkin, T. Kaper, and A. Nadim. Coupled pulsation and translation of two gas bubbles in a liquid. *Journal of Fluid Mechanics*, 445:377–411, 2001.

[20] Institute of Acoustics. *From Sea to Surgeries, from Babbling Brooks to to Baby Scans: Bubble Acoustics at ISVR*, volume 26, 2004.

[21] T. Kalmár-Nagy, G. Stépán, and F. C. Moon. Subcritical hopf bifurcation in the delay equation model for machine tool vibrations. *Nonlinear Dynamics*, 26:121–142, 2001.

[22] J. B. Keller and I. I. Kolodner. Damping of underwater explosion bubble oscillations. *Journal of Applied Physics*, 27:1152–1161, 1956.

[23] J.B. Keller and M. Miksis. Bubble oscillations of large amplitude. *Journal of the Acoustical Society of America*, 68:628–633, 1980.

[24] Yuri A. Kuznetsov. *Elements of Applied Bifurcation Theory*. Springer, 3 edition, 2004.

[25] W. Lauterborn and T. Kurz, editors. *Dynamics of Delay-Coupled Spherical Bubbles*. 15th International Symposium on Nonlinear Acoustics, 1999.

[26] W. Lauterborn and U. Parlitz. Methods of chaos physics and their application to acoustics. *Journal of the Acoustical Society of America*, 84:1975–1993, 1988.

[27] S. Ma, Q. Lu, and Z. Feng. Double hopf bifurcation for van der pol-duffing oscillator with parametric delay feedback control. *Journal of Analysis and Applications*, 338:993–1007, 2008.

[28] R. Manasseh, A. Nikolovska, A. Ooi, and S. Yoshida. Anisotropy in the sound field generated by a bubble chain. *Journal of Sound and Vibration*, 278:807–812, 2004.

[29] M. S. Plesset and A. Prosperetti. The dynamics of cavitation bubbles. *Journal of Applied Mechanics*, 16:277–282, 1949.

[30] M. S. Plesset and A. Prosperetti. Bubble dynamics and cavitation. *Annual Review of Fluid Mechanics*, 9:145–85, 1977.

[31] R. H. Rand. *Topics in nonlinear dynamics with computer algebra*. Langhorne, PA: Gordon and Breach Science Publishers, 1994.

[32] R. H. Rand. *Complex Systems: Fractionality, Time-delay and Synchronization*, chapter Differential-Delay Equations, pages 83–117. Springer, 2011.

[33] R. H. Rand. Lecture notes on nonlinear vibrations (version 53). `http://ecommons.library.cornell.edu/handle/1813/28989`, 2012.

[34] R. H. Rand and D. Armbruster. *Perturbation methods, bifurcation theory, and computer algebra*. Springer-Verlag New York, 1987.

[35] Lord Rayleigh. On the pressure developed in a liquid during the collapse of a spherical cavity. *Phil. Mag.*, 34:94–98, 1917.

[36] A. J. Reddy and A. J. Szeri. Coupled dynamics of translation and collapse of acoustically driven microbubbles. *Journal of the Acoustical Society of America*, 112:1346–1352, 2002.

[37] M. K. Suchorsky, S. M. Sah, and R. H. Rand. Using delay to quench undesirable vibrations. *Nonlinear Dynamics*, 62:107–116, 2010.

[38] J. O. Toilliez and A. J. Szeri. Optimized translation of microbubbles driven by acoustic fields. *Journal of the Acoustical Society of America*, 123:1916–1930, 2008.

[39] S. Wirkus and R. H. Rand. Dynamics of two coupled van der pol oscillators with delay coupling. *Nonlinear Dynamics*, 30:205–221, 2002.

[40] J. Xu, K. W. Chung, and C. L. Chan. An efficient method for studying weak resonant double hopf bifurcation in nonlinear systems with delayed feedbacks. *SIAM Journal of Applied Dynamical Systems*, 6:29–60, 2007.

[41] Y. Yamakoshi, Y. Ozawa, M. Ida, and N. Masuda. Effects of bjerknes forces on gas-filled microbubble trapping by ultrasonic waves. *Japanese Journal of Applied Physics*, 40:3852–3855, 2001.

[42] P. Yu, Y. Yuan, and J. Xu. Study of double hopf bifurcation and chaos for an oscillator with time delayed feedback. *Communications in Nonlinear Science and Numerical Simulation*, 7:69–91, 2002.